nature reviews methods primers

https://doi.org/10.1038/s43586-023-00257-4

Primer

Check for updates

Finite-difference time-domain methods

F. L. Teixeira[1], C. Sarris[2], Y. Zhang[3], D.-Y. Na[4], J.-P. Berenger[5], Y. Su[6], M. Okoniewski[7], W. C. Chew[8], V. Backman[6] & J. J. Simpson[3]

Abstract

The finite-difference time-domain (FDTD) method is a widespread numerical tool for full-wave analysis of electromagnetic fields in complex media and for detailed geometries. Applications of the FDTD method cover a range of time and spatial scales, extending from subatomic to galactic lengths and from classical to quantum physics. Technology areas that benefit from the FDTD method include biomedicine — bioimaging, biophotonics, bioelectronics and biosensors; geophysics — remote sensing, communications, space weather hazards and geolocation; metamaterials — sub-wavelength focusing lenses, electromagnetic cloaks and continuously scanning leaky-wave antennas; optics — diffractive optical elements, photonic bandgap structures, photonic crystal waveguides and ring-resonator devices; plasmonics — plasmonic waveguides and antennas; and quantum applications — quantum devices and quantum radar. This Primer summarizes the main features of the FDTD method, along with key extensions that enable accurate solutions to be obtained for different research questions. Additionally, hardware considerations are discussed, plus examples of how to extract magnitude and phase data, Brillouin diagrams and scattering parameters from the output of an FDTD model. The Primer ends with a discussion of ongoing challenges and opportunities to further enhance the FDTD method for current and future applications.

Sections

Introduction

Experimentation

Results

Applications

Reproducibility and data deposition

Limitations and optimizations

Outlook

[1]Department of Electrical and Computer Engineering, The Ohio State University, Columbus, OH, USA. [2]Department of Electrical and Computer Engineering, University of Toronto, Toronto, Ontario, Canada. [3]Department of Electrical and Computer Engineering, University of Utah, Salt Lake City, UT, USA. [4]Department of Electrical Engineering, Pohang University of Science and Technology, Pohang, Korea. [5]Department of Electrical and Electronic Engineering, The University of Manchester, Manchester, UK. [6]Biomedical Engineering Department, Northwestern University, Evanston, IL, USA. [7]Department of Electrical and Software Engineering, University of Calgary, Calgary, Canada. [8]Department of Electrical and Computer Engineering, Purdue University, West Lafayette, IN, USA. e-mail: jamesina.simpson@utah.edu

Introduction

As one of the four fundamental forces of nature, electromagnetic fields are ubiquitous in the natural environment and modern technologies. The field of electromagnetics began with discoveries into static electricity and the magnetic field of the Earth and has expanded to include a range of scientific disciplines and engineering applications, such as wireless radio communications, biomedical imaging and quantum technologies. Fundamental to these advances was the formation of Maxwell's equations in 1865 (ref. 1) as well as the development of robust and powerful solutions to those equations. The reason Maxwell's equations and their solutions endure is that they are valid from subatomic to galactic length scales and from classical to quantum physics[2].

Initial efforts focused on obtaining exact solutions to Maxwell's equations for canonical geometries. During this time, the Sommerfeld integral, Rayleigh scattering, Mie scattering[3] and the Debye model[4] were pioneered. This was followed by an era of approximate solutions[4], including geometrical optics, asymptotic theory, the geometrical theory of diffraction and perturbational techniques. With the advent of the modern computer, numerical solutions started to appear.

Compared with exact or approximate analytical approaches, numerical techniques provide greater flexibility and can consider more complex scenarios. The early focus on the frequency domain meant that, initially, numerical solutions to Maxwell's equations were only obtained in the frequency domain.

A robust numerical method for solving Maxwell's equations was finally formulated in the time domain with the introduction of the finite-difference time-domain (FDTD) method in 1966 (ref. 5). The approach decomposes the spatial domain of interest into grid cells, in which each grid cell has staggered electric and magnetic field components, as shown for Cartesian coordinates in Fig. 1a.

The FDTD method has several advantages. It evolves in time, just as nature evolves over time. As a result, FDTD results can give a direct insight into the time evolution of electromagnetic fields. The models are matrix-free and may be efficiently parallelized onto supercomputers in a straightforward manner. Additionally, the FDTD method treats impulsive and nonlinear behaviour naturally, although sources of error are well understood and may be bounded to certain tolerance levels. Finally, FDTD models do not automatically need to be reformulated for different problems. Instead, changes are typically only made to account for additional physics as needed.

Before choosing the FDTD method, it is important to note its disadvantages. FDTD simulations are relatively slow because the Courant–Friedrichs–Lewy (CFL) condition[6] must be satisfied to maintain stability. Typically, the grid cell dimensions — $\Delta x\,\Delta y$ and Δz in Cartesian coordinates — are chosen to satisfy the geometrical details of interest and have at least 10–20 grid cells per shortest electromagnetic wavelength for sufficient accuracy[7]. On the basis of these grid cell sizes, the time-step increment is chosen that satisfies the CFL condition. For cubic grid cells of dimensions $\Delta x = \Delta y = \Delta z = \Delta$, the CFL condition reads $\Delta t \leq \frac{\Delta}{c\sqrt{3}}$, in which c is the speed of light. Furthermore, the FDTD method is sensitive to the shape and size of grid cells. As a result, FDTD models usually have uniformly shaped grid cells that may cause defeaturing of certain geometries. However, there are techniques to model material boundaries inside a grid cell and features smaller than a grid cell, such as thin wires. Additionally, not all electromagnetic field component values — especially those required for implementing complex materials — are directly solved for by the algorithm at the required locations and timepoints. This can sometimes lead to stability issues. Despite these disadvantages, the FDTD method continues to grow in popularity because it is robust, flexible and relatively easy to implement.

This Primer provides an overview of FDTD modelling capabilities applied to various applications across the electromagnetic spectrum. It concludes with an outlook on future possibilities.

Experimentation

The FDTD method solves the time-domain form of Faraday's law and Ampere–Maxwell's law to obtain the time evolution of electric and magnetic fields across a spatial grid. Originally, the FDTD method was proposed using the differential forms of Faraday's and Ampere–Maxwell's laws:

$$\text{Faraday's law}: \mu\frac{\partial \mathbf{H}}{\partial t} = -\nabla \times \mathbf{E} - \mathbf{M}, \tag{1}$$

$$\text{Ampere} - \text{Maxwell's law}: \varepsilon\frac{\partial \mathbf{E}}{\partial t} = \nabla \times \mathbf{H} - \mathbf{J}_s - \sigma\mathbf{E}, \tag{2}$$

in which $\mathbf{E}$ is the electric field, $\mathbf{H}$ is the magnetic field, $\mathbf{J}_s$ represents an electric current density source and $\mathbf{M}$ is the equivalent magnetic current density. Three primary constitutive parameters are used to describe the electromagnetic properties of materials: ε, electric permittivity; μ, magnetic permeability and σ, conductivity. Materials and objects of interest are generally placed into the grid by assigning constitutive material parameters on the basis of the cell location.

FDTD grids are typically generated in Cartesian coordinates using non-collocated, staggered electric and magnetic field components, as shown in Fig. 1a. Central differencing is used to approximate the time and spatial partial derivatives in equations (1) and (2). Truncating the Taylor series expansions of the field components yields a second-order accurate scheme in both space and time.

There are numerous source options for an FDTD model. These include hard, soft, resistive voltage and plane wave sources. Hard sources have field components set at specific locations to specific time waveforms and are the simplest source option. However, hard sources are non-physical and scatter incoming electromagnetic waves. Current or soft sources that are implemented by assigning values to the $\mathbf{J}_s$ term in Ampere–Maxwell's law (equation (2)) are used to account for current flow in the model. They are useful for modelling impressed sources that do not perturb the underlying electromagnetic response (Green's function) of the problem. Resistive voltage sources[7] can simulate sources with prescribed impedance profiles, such as at the feeding point of an antenna. Plane waves from a distant source may be efficiently modelled using a perfectly matched total-field scattered-field formulation[8]. Using the perfectly matched total-field scattered-field formulation, the numerical dispersion introduced by the FDTD grid is accounted for in the incident wave calculation. As a result, the addition or subtraction of the incident wave in the FDTD model is accurate down to machine precision.

Alongside an appropriate source, all FDTD models must have suitable boundary conditions. Candidate boundary conditions include perfect electric conductor (PEC); perfect magnetic conductor (PMC); periodic boundary conditions (PBCs); surface impedance boundary conditions (SIBCs); and absorbing or radiation boundary conditions. PEC and PMC facets reflect electromagnetic waves and are the simplest boundary conditions. They are only appropriate for modelling (high conductivity) metallic structures at or below microwave frequencies (PEC) or to take advantage of certain types of symmetries in the

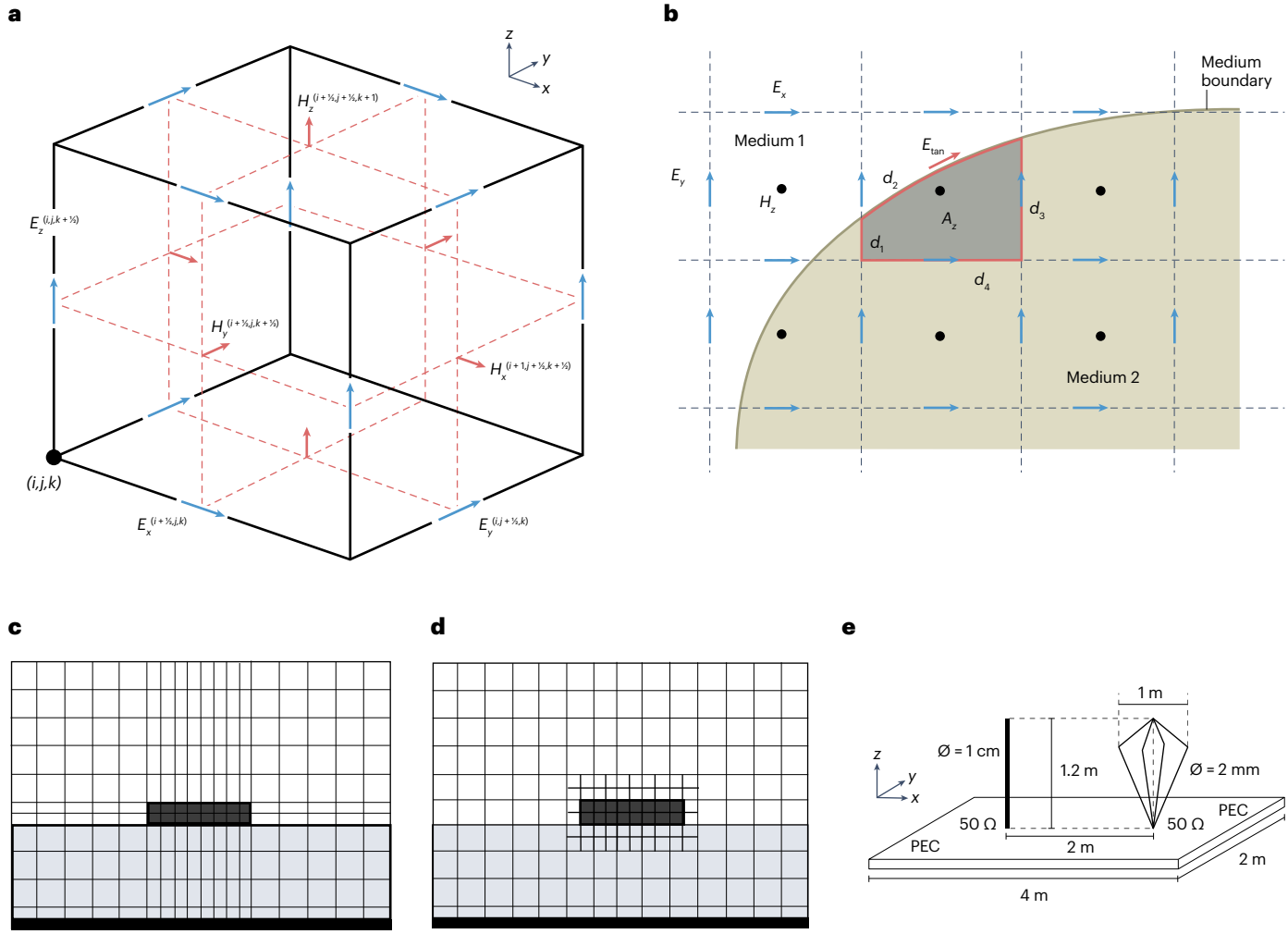

Fig. 1 | Details for common finite-difference time-domain grid arrangements. **a**, A 3D finite-difference time-domain (FDTD) (Yee) grid cell in Cartesian spatial coordinates. The grid cell has dimensions $\Delta x \times \Delta y \times \Delta z$ in space, with staggered electric and magnetic field components oriented in each Cartesian direction. i, j, k are grid cell indices for the x-direction, y-direction and z-direction, respectively. **b**, Staircasing in an FDTD model comprised of regular, square Cartesian grid cells arising from the grid electromagnetic components not lining up with the material boundary. A locally conformal FDTD algorithm is applied to one grid cell containing the curved object. **c**, A non-uniform gridding approach for an FDTD grid refinement applied to a thin microstrip line printed on a dielectric substrate. Higher resolution is needed to accurately model the fringing fields around the edges of the metallic strip. **d**, Same as part **c**, but with a subgrid instead of non-uniform gridding. **e**, Example of thin-wire antennas modelled in an FDTD grid. A monopole antenna and conical antenna on a 400 × 200 × 10-cm perfect electric conductor (PEC) plate. The structure is illuminated by a plane wave. The FDTD grid resolution is $\Delta x = \Delta y = \Delta z = 5$ cm and the time-step increment $\Delta t = 0.075$ ns. The monopole is modelled as a thin wire (diameter $\phi = 1$ cm) parallel to the z-direction (120-cm long, spanning 24 cells). The conical antenna is modelled using nine straight thin wires ($\phi = 2$ mm) connected to form the wire structure: one short vertical wire (5-cm long, spanning one grid cell) and eight oblique wires (four wires of 21 cells 5.11-cm long and four wires of 11 cells 4.90-cm long). Both antennas are connected to the PEC plate through a 50-Ω resistor.

problem (PEC and PMC). PBCs[9,10] connect opposite edges of the grid to each other. This boundary condition is suitable when a structure is periodic — such as phased antenna arrays, photonic crystals and metamaterials — and to approximate a geometry that should appear to continue beyond the edges of the computational domain, for instance, when approximating the ionosphere as extending far beyond the FDTD grid[11]. SIBC avoids the need to extend a model into a material, which usually requires smaller grid cell sizes owing to the reduced electromagnetic wavelength[12,13]. Both frequency-independent and frequency-dependent SIBC formulations are available. Absorbing or radiation boundary conditions are suitable for open-region problems, in which surrounding objects may be ignored in the simulation because they are sufficiently far away from the FDTD grid or not of direct interest. Radiation boundary conditions are used infrequently, for example, when absorbing boundary conditions exhibit stability issues, such as for magnetized plasma.

The perfectly matched layer

The main goal of any absorbing boundary condition is to minimize spurious reflections along the outer boundaries of the grid. The perfectly

matched layer (PML)[14,15] is the most popular absorbing boundary condition for the FDTD method owing to its overall efficiency, low reflection levels, robustness, relative ease of implementation and flexibility.

After the PML was originally introduced, it was reformulated as a complex-valued mapping applied to the spatial coordinates[16–18]. This led to the PML version most commonly used today, which uses transformation optics principles applied to Maxwell's equations[19]. The coordinate mapping is fully recast as modified, permeability and permittivity tensors into the original, real-valued, coordinate domain. The form of Maxwell's equations is preserved via an anisotropic and dispersive medium — or an artificial PML medium — also known as uniaxial PML[17,20]. Consequently, algorithms for implementing the FDTD method in anisotropic and dispersive media may be retooled for PML media in an FDTD model and vice versa[21–23].

Complex media

Beyond simple linear materials with scalar constitutive relations, the FDTD method has been successfully applied to a large class of dispersive, anisotropic and nonlinear materials. These include dispersive, frequency-dependent materials, such as Drude, Lorentz, Debye and gyromagnetic materials, for example, magnetized ferrites and plasma. Two main approaches have been applied. The first approach involves numerical integration of the time convolution integrals. The exponential nature of the susceptibility functions is exploited to avoid storing the entire time history of the fields. In its place, recursive accumulators are used so that only a few past time-step field values are required in the FDTD update equations[24,25]. The second approach involves auxiliary differential equations. Here, additional differential equations, which represent the physics of the material, are solved simultaneously with Maxwell's equations[24,26]. Examples include magnetized ferrites[27,28] and magnetized plasma[29]. The constitutive parameters of the dispersive media should be obtained[30,31] before the FDTD implementation. It is also possible to implement dispersive media using a Z-transform approach[32,33].

In anisotropic media, the constitutive parameters are represented as tensors. Several FDTD extensions have been successfully developed to handle anisotropic media[34–37]. An important example of anisotropic media is the PML media[18,19]. In nonlinear media, the constitutive parameters depend on the electric or magnetic field strengths. Constitutive relations for a nonlinear medium are expressed in terms of nonlinear susceptibilities, in addition to linear susceptibilities[38,39]. Special cases of nonlinear susceptibilities include isotropic models, such as the Kerr model with a quadratic dependency of the permittivity on the electric field strength, and the cubic-quintic Kerr model with both quadratic and quartic dependencies[24]. The implementation of nonlinear media in FDTD is accomplished by either an iterative loop or a root-finding algorithm, such as Newton–Raphson's algorithm applied within each time step[24]. These approaches may be adapted to integrate nonlinear lumped circuit elements — diodes, transistors and other semiconductor devices — into FDTD simulations[34]. In several multiphysics problems, Maxwell's equations do not constitute a closed system and the constitutive relations will not fully capture all the dynamic effects. In such cases, the FDTD algorithm should be integrated as a field solver, with the set of equations discretizing the coupled dynamics[40,41]. Special care must be taken to minimize numerical FDTD artefacts that might subtly affect the behaviour of the coupled dynamics[42,43].

Spatial gridding

Complex geometries. Each grid cell of an FDTD model must be assigned material constitutive properties. It is common to use uniform grid cells that are rectangular or cubic, meaning that complex geometries may not always be replicated, producing a staircase error. This may be seen in Fig. 1b, in which the material boundary does not line up with the grid cell edges.

To mitigate staircasing errors, locally conformal FDTD grid implementations may be used, in which the FDTD grid cells are deformed next to curved or sloped boundaries[25,44–46]. Although locally conformal FDTD algorithms produce more accurate results for problems with curved and sloped geometries, their implementation requires additional bookkeeping to handle the local geometric features. Extra care is needed to avoid numerical instabilities[47].

For problems involving highly complex 3D structures, manually creating the FDTD grid according to the object shape may be costly and error prone. To avoid these problems, automatic grid generation techniques based on input computer-aided design files and computer graphics principles[48] may be used.

Subcell models and subgridding. Many geometries contain localized geometric details and strong, localized fields. Consider, for example, an array of plasmonic nanospheres embedded in a dielectric host medium. Plasmonic modes may be strongly localized on the surface of the nanospheres, in which the geometry does not conform to a grid of rectangular Yee grid cells. Therefore, grid refinement is necessary to accurately simulate these structures and capture surface field resonances.

There are four possibilities for implementing a grid refinement. The first, brute-force approach involves uniformly applying the minimum cell size required anywhere in the computational domain. This approach is simple to implement. However, it results in a large computational overhead. A second option is to use non-uniform gridding, as shown in Fig. 1c, in which only a fraction of the cells are refined[49,50].

A third option is a subcell method, in which the cell size is maintained, but effective material parameters are assigned to the cell to account for material boundaries within the cells[51]. These parameters may be scalar or tensorial[52,53] and may also account for the dispersive properties of materials[46,54,55].

Subgridding, shown in Fig. 1d, is the most advanced technique. Grids of different resolutions are coupled together via a set of update equations, independent of the regular finite differences for Maxwell's equations[56–58]. These interface update equations may result in a late-time instability[59] but consistent formulations have been presented to ensure that subgrids are coupled in a stable fashion[60–62].

FDTD subgridding methods may be categorized on the basis of how they treat time-stepping, as subgrids reduce the required time-stepping increment. To meet this stability constraint, two methods have been developed. The first uses a uniformly reduced time step on the basis of the CFL condition for the densest subgrid. The second uses adaptive time-stepping, in which subgrids are assigned time-step increments according to their own CFL condition and the subgrids and coarse mesh are synchronized through temporal interpolations and extrapolations[59,62].

Thin-wire models. The thin-wire formalism is an important subcell model that allows wires thinner than the grid cell dimensions to be accounted for in an FDTD model. Straight wires of arbitrary radius, length and orientation may be implemented[63]. Furthermore, wires may be placed anywhere in the domain, even independent of the FDTD grid cell features. Sources and loads may be connected to wires to form circuits. FDTD grid cells may be comprised of both thin wires and any other objects.

The basic methodology of the thin-wire method involves solving a set of partial differential equations for each straight wire using the 1D FDTD method in parallel with conventional FDTD solution for Maxwell equations[63,64]. Each wire is discretized independently from the rest of the model. The chosen spatial discretization of any wire should not be too large to obtain accurate sampling of the current and charge distribution of the wire. It also must not be too small, as the 1D solution on the wire is also subject to the CFL stability condition.

Figure 1e illustrates some possibilities of the thin-wire formalism through a canonical example that includes a two-cell thick PEC plate along with two thin-wire antennas in the same FDTD domain.

Cylindrical and spherical FDTD models. For problems with cylindrical or spherical symmetries, it is desirable to use cylindrical and spherical FDTD grids that are conformal to the geometries of interest. These grids may mitigate staircasing errors and remove the need for high grid resolutions or locally conformal implementations[35,65]. In cylindrical and spherical coordinates, the finite-difference approximations for the spatial derivatives must properly account for the changing metric factors. They also require special treatment of the coordinate singularities along the axis of symmetry or on the spherical poles. Cylindrical and spherical FDTD algorithms are routinely used for diverse applications such as optics[66], geophysics[67,68] and ionospheric propagation[69,70].

Non-orthogonal and unstructured FDTD models. The FDTD method can be extended to non-orthogonal curvilinear grids, increasing the geometric flexibility beyond regular Cartesian, cylindrical and spherical grids. In this case, the FDTD grids are comprised of deformed quasi-hexahedral cells[65–68]. A field representation in terms of covariant and contravariant field components may be used to account for grid cell deformation and non-orthogonality[68].

Alternatively, FDTD extensions can be obtained on the basis of a finite-element framework. The conventional FDTD algorithm is equivalent to a Galerkin-type finite-element time domain (FETD) algorithm on a Cartesian grid using mixed face or edge basis functions and low-order quadrature rules[71]. Although this approach is suitable for handling arbitrarily shaped geometries, conventional FETD requires a linear system of equations to be solved in each time step, which is less efficient than the FDTD method. Nevertheless, there are advantages of constructing FDTD schemes on more general grids on the basis of finite-element principles[72–74].

Unconditionally stable FDTD methods

The conventional FDTD algorithm is conditionally stable because the time-step increment is constrained by the CFL condition. It is possible to construct unconditionally stable FDTD methods on the basis of modifying the time-stepping algorithm used for field updates[75,76]. The Newmark-β FDTD algorithm[77] and the Crank–Nicolson FDTD algorithm[78] are two popular methods. Unconditionally stable methods are particularly useful for problems that require very fine grid resolutions of two or more orders of magnitude less than the wavelength[40].

Unconditionally stable methods have drawbacks. The field values to be solved at any given time step depend on known past field values and unknown present field values at other grid points. The result is an implicit time update that requires solution of a sparse matrix equation at each time step to obtain the next field value. Additionally, the condition number of the underlying system matrix tends to grow with time-step size[79]. This leads to a slower field update for schemes that use iterative solvers for the sparse matrix equation.

Dimensional splitting unconditionally stable algorithms, such as the alternating direction implicit and the locally one-dimensional algorithms, involve only tridiagonal matrices and require iterative solvers at each time step. Alternating direction implicit-FDTD[80–82] and locally one dimensional-FDTD[83,84] introduce additional splitting errors. Care must be exercised when choosing the simulation parameters to ensure that the numerical error remains within acceptable bounds.

Parallel computing and hardware acceleration

Conventional FDTD is formally an Iterative Stencil Loops simulator or a time marching, finely grained, nearest neighbour algorithm. It is an explicit algorithm, in which new field values are computed using only previously computed field components. These characteristics make FDTD models highly parallel and well suited to various parallel computational hardware components, from mainstream multicore central processing unit (CPU) chips and graphical processing unit (GPU) chips[85], to special-purpose hardware based on field programmable gate arrays. As of 2023, multicore CPUs and GPUs are the two main computational hardware platforms available to an FDTD developer.

Contemporary CPUs have up to 24 or 64 cores. From the perspective of a programmer, each core is a fully functioning processor that splits each core into two virtual cores, called threads. A single 18-core CPU may run 36 threads or independent processes. For the FDTD method, developers may achieve effective parallelization by using OpenMP API with a simple parallelization pragma added in front of the nested loops with field updates. If more complex field updates are required in a small area — for example, complex materials or subcell models — it is beneficial not to break the parallel loops. Instead, a backward time step can be performed and the field recomputed using updates, reflecting the local field interaction complexity.

By contrast, GPUs are massively parallel computational platforms. The highly parallel sections of the code are executed on the GPU device as kernels. A kernel executes in parallel across a set of threads, organized into thread blocks and arranged into a grid. To execute kernels, thread blocks are distributed across streaming multiprocessors on the basis of resource availability. Multiple instructions, multiple data may be executed across a thread processing cluster, with single instruction multiple data on each streaming multiprocessor.

A GPU FDTD programmer does not use loops to update fields. Instead, the simulation domain is divided into blocks of FDTD cells to be distributed across thread processors. Computing fields at the edge of the block requires data from neighbouring blocks at every time step.

At the time of writing, a single NVIDIA Hopper GPU has 80 GB of high-speed memory, and 18,176 CUDA cores, each with 2 floating point units. This resource enables large FDTD simulations with more than 3 billion grid cells, for example, a photonics problem with grid dimensions of 6,000 × 6,000 × 90, or an antenna problem with grid dimensions of 1,500 × 1,500 × 1,400. High-end PC machines can support multiple GPU cards. Message passing interface may be used to extend parallelization to multiple GPUs and machine clusters, which each have multiple GPUs. Most commercial FDTD codes can use a single GPU at minimum.

Higher-order FDTD modelling

The accuracy of the FDTD method for electrically large problems, which span many tens of wavelengths or more, is primarily limited by numerical or grid dispersion. This causes the phase velocity of the waves in the FDTD grid to exhibit spurious variations versus both frequency (dispersion) and propagation (anisotropy) angle.

Glossary

Boundary conditions
Description of the behaviour of the solutions at certain points in space, usually along the outer edges of the finite-difference time-domain grid.

Courant–Friedrichs–Lewy (CFL) condition
A constraint that must be satisfied to achieve convergence and maintain numerical stability in a simulation.

Iterative Stencil Loops simulator
A numerical data processing solution where an array of elements is updated according to a fixed pattern called a stencil.

Maxwell's equations
Two coupled partial differential equations that govern the propagation of electromagnetic waves.

Monte Carlo method
When applied to the finite-difference time-domain method, the Monte Carlo method involves rerunning a finite-difference time-domain simulation numerous times, often thousands or millions of times, to obtain a range of possible electric or magnetic field outcomes for an uncertain modelling scenario.

Scattering parameters
S-parameters provide a relationship between the input and output of an electrical network.

Higher-order FDTD algorithms may be used to reduce the numerical dispersion. Conventional higher-order FDTD algorithms are based on extended finite-difference stencils to approximate the field derivatives[86]. This is often denoted as (n,p) FDTD, in which n and p refer to the order of the truncation error in time and space, respectively. Using this notation, the conventional second-order FDTD algorithm, Yee's scheme, is (2,2) FDTD. The (2,4) FDTD algorithm strikes a good balance between accuracy and computational cost[87].

The main limitation of higher-order schemes comes from the behaviour of larger spatial stencils across material interfaces, in which the higher order of the finite-difference approximation is not retained. Although approaches are available to maintain the accuracy order of higher-order FDTD schemes across interfaces[88,89], they are characterized by a decrease in generality and a substantial increase in the implementation complexity.

In broadband problems, grid dispersion effects are exacerbated at the high end of the frequency band. The phase error may be more uniformly minimized across a wide frequency band by modifying the coefficients of the enlarged finite-difference stencils[90–92]. Figure 2a provides a notional view of the most suitable FDTD algorithms according to the electrical size of the problem domain and chosen grid resolution.

Scientific machine learning

Deep learning methods have been developed as alternatives to conventional numerical techniques for solving partial differential equations and inverse problems. Developments include physics-informed neural networks (PINNs)[93,94], the deep Galerkin method[95] and deep Ritz method[96]. These methods do not explicitly use any spatial or temporal discretization. As a result, they are not subject to the numerical dispersion and stability constraints of the FDTD method. Instead, the PINN-based solution of Maxwell's equations relies on minimization of a loss function that represents how well the generated data satisfy the equation, along with its initial and boundary conditions.

In ref. 97, a fully connected artificial neural network, with a loss function evaluated by automatic differentiation, was used to simulate wave propagation in inhomogeneous and nonlinear media, replicating the FDTD solution with excellent accuracy. Alternatively, the loss function may be evaluated on an FDTD grid using finite differences to approximate the derivatives. This approach was followed by ref. 98 for coupled electromagnetic-thermal simulations.

A supervised strategy, using a convolutional neural network (CNN) and a long short-term memory (LSTM) network trained with FDTD data, was used in ref. 99 to rapidly extract the scattering parameters of various planar microwave structures. The CNN processed the geometry of the simulated structure, whereas the LSTM processed the scattering parameters computed by a coarse-mesh FDTD simulation. The hybrid CNN–LSTM network rapidly and accurately computed the scattering parameters of new structures not previously seen by the networks, in a fraction of the simulated time needed for a dense grid FDTD simulation. A flowchart of this approach is shown in Fig. 2c.

The current state of the art still requires significant computational resources for off-line training of neural network models. This is achieved either by using ground-truth FDTD data[99] or via the PINN approach of minimizing a cost function on the basis of the equations to be solved[97,98]. Such models are efficient surrogates of FDTD in scenarios that need repetitive simulations, for instance, design optimization, uncertainty quantification and yield analysis. They should not be seen as replacements of FDTD models or standalone simulators.

Results

The electromagnetic fields predicted in space and time by FDTD models are ideal for generating animations of the field behaviour. When dealing with large or long models running on supercomputers, parallel input and output — such as HDF5[100] — is highly beneficial to save the desired output data. When sampling a field component in space, the field values are averages over the full dimensions of a grid cell, even though they are typically drawn (as in Fig. 1a) or stored (in computer memory) in a manner that implies that the field components are located at just one specific position in space.

When the spectrum of a field component is desired, a post-run discrete Fourier transform (DFT) may be applied to the data. For simulations involving a large number of time steps, an on-the-fly DFT may be performed within the time-stepping loop[7]. To avoid any artificial high frequency components, the DFT should be performed either on results that decay to zero or until the data reach a zero-crossing.

Overall, it is good practice to validate new FDTD models or new algorithmic approaches against available analytical results, measurement data, other computational approaches or previous FDTD models such as convergence studies. This helps to confirm the validity of the model before applying it to new problems. For example, if the grid resolution is doubled and the model predicts analogous electromagnetic fields, it is assumed that the results have converged.

Uncertainty quantification

Many devices and systems of interest have uncertainties owing to tolerances in the manufacturing process, statistical fluctuations of material properties or changes in environmental conditions. These uncertainties mean that the output response of a model is also statistically variable. Quantifying this statistical variability is important to establish reliable models with realistic design margins for robust optimization. Uncertainty quantification addresses this challenge.

Various uncertainty quantification methods have been integrated with FDTD, across a range of applications. For example, the Monte Carlo method was used to evaluate scattering from rough surfaces in ref. 101.

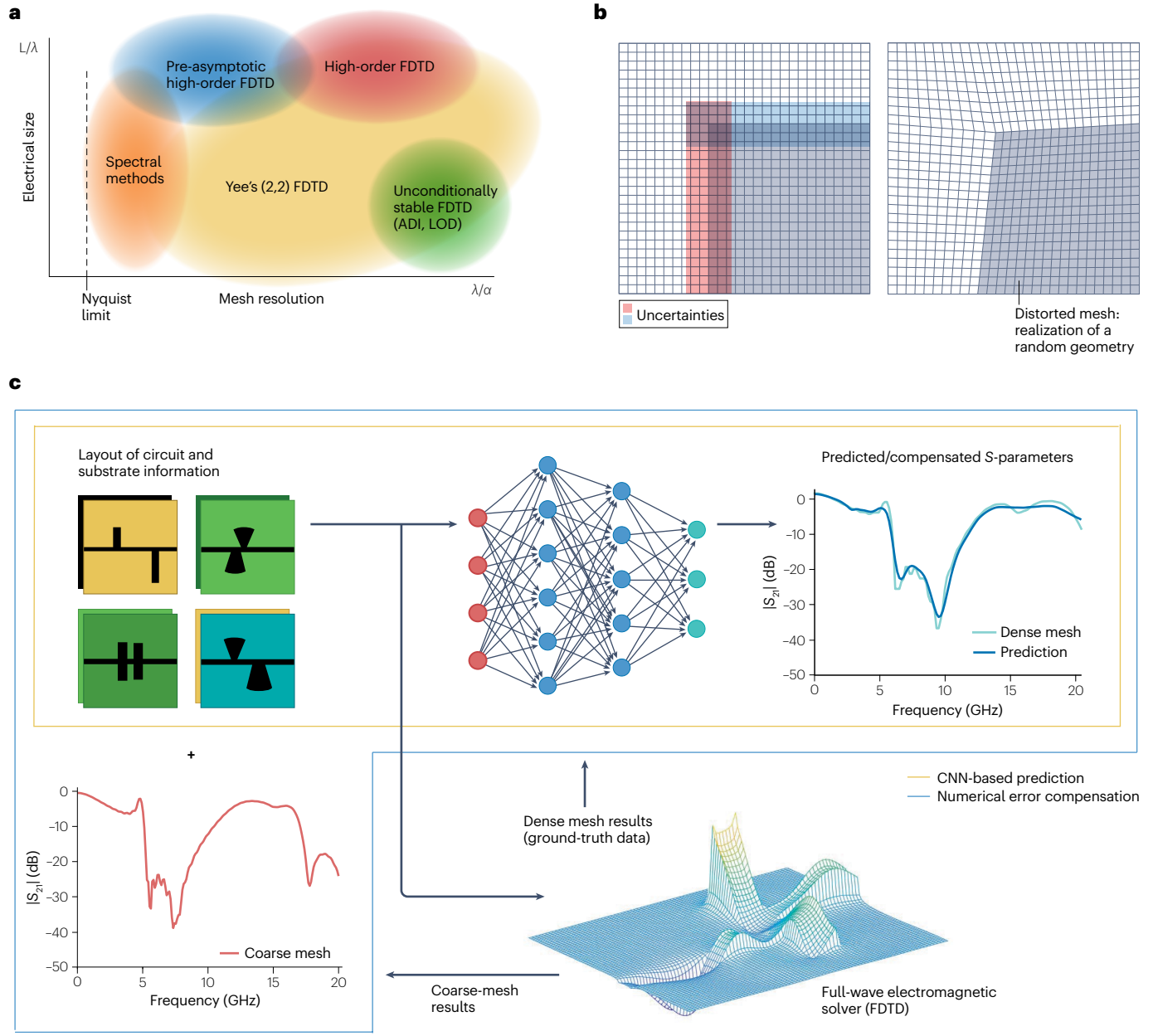

Fig. 2 | Advanced finite-difference time-domain modelling approaches. **a**, Suitable finite-difference time-domain (FDTD) algorithms, depending on the electrical size of the problem, the FDTD grid and the chosen grid resolution. Spectral methods use a Fourier transform to represent spatial derivatives. **b**, Example of a stochastically deformable, generalized curvilinear computational grid applied at a metallic edge having a statistically variable geometry. **c**, Example flowchart for a supervised training method, in which a convolutional neural network (CNN) network uses the information from the geometry image and a long short-term memory network uses the coarse FDTD data. This method is used to rapidly produce the scattering parameters of planar microwave structures over a broad bandwidth (0–20 GHz). α, FDTD cell size; λ, wavelength; ADI, alternating direction implicit; L, domain size; LOD, locally one dimensional. Part **b** adapted with permission from ref. 105, IEEE. Part **c** reprinted with permission from ref. 99, IEEE.

The Monte Carlo method is simple to implement, versatile and non-intrusive as it is based on post-processing iterative simulations. However, the statistics — mean and variance — converge at a rate proportional to $1/\sqrt{N}$, where N is the number of simulations[102]. This limits the Monte Carlo method when applied to computationally large problems.

Methods that use polynomial chaos expansion (PCE) have been formulated as robust alternatives to Monte Carlo. PCE is based on expanding the output function of interest, a second-order random process, as orthogonal polynomials of the random input parameters[103]. A major challenge is that the number of polynomials grows with the number of random input parameters and polynomial order.

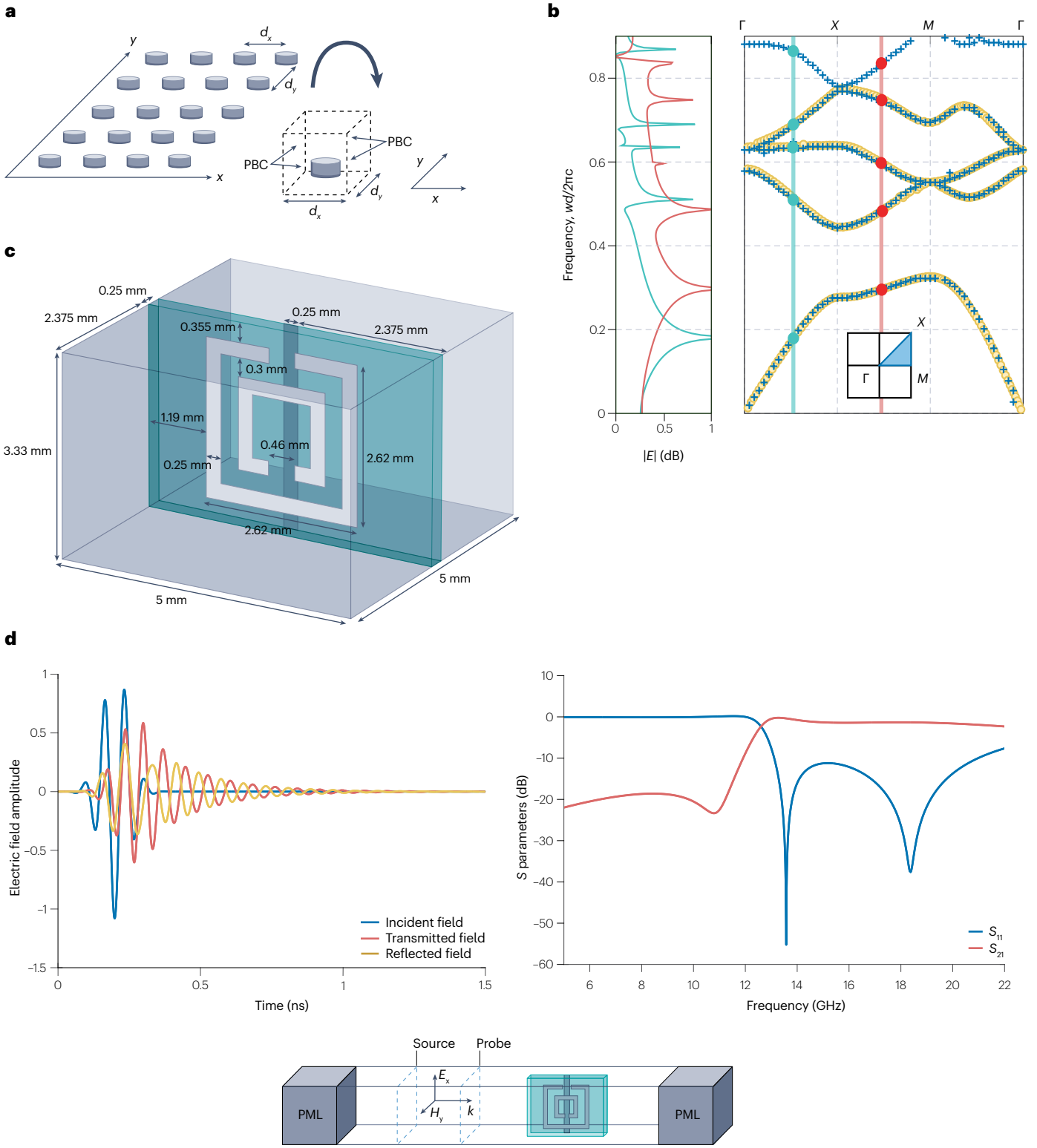

The expansion coefficients in PCE may be determined with a non-intrusive procedure by post-processing multiple FDTD simulations at a set of input parameter vectors[104]. Alternatively, intrusive implementation starts by expanding all field components in terms of polynomials of the random inputs and recasting the entire system of FDTD updates as a set of equations with respect to the field expansion

Fig. 3 | Example approaches for obtaining results from finite-difference time-domain simulations. A band diagram (panels **a** and **b**) and *S*-parameters (panels **c** and **d**). **a**, A 2D lattice of cylinders. The periodic array is reduced to a single unit cell modelled in an finite-difference time-domain (FDTD) grid via periodic boundary conditions. Within the unit cell, a broadband source excitation — such a Gaussian source — excites electromagnetic waves, whose frequency spectra consist of peaks at the resonant frequencies corresponding to the wavevector **k** enforced by the periodic boundary conditions (PBCs). The maximum simulated frequency of interest is f_{max} = 15 GHz and the spatial resolution corresponds to 20 cells per wavelength in each direction at f_{max}. Twenty samples of the wavevector are taken between each edge of the Brillouin zone. The time step is 0.9 of the Courant–Friedrichs–Lewy limit and each PBC-based simulation runs for 8,192 time steps. **b**, Right: Brillouin (band) diagram for the square lattice of aluminium cylinders with period d = 2 cm computed by the FDTD method (crosses) and data from ref. 207 (thick yellow lines). Left: the magnitude of the Fourier transform of the electric field sampled within the unit cell for two wavevectors within the irreducible Brillouin zone. The detected peaks are transferred to the band diagram and shown with green and red dots, respectively. **c**, The geometry of a split ring resonator/strip wire unit cell. **d**, Computational domain of the FDTD simulation, incident/reflected/transmitted electric field time-domain waveforms and scattering parameters of the split ring resonator/strip wire unit cell. PML, perfectly matched layer. Parts **c** and **d** reprinted with permission from ref. 119, IEEE.

coefficients. In this case, a curse of dimensionality translates to more update equations. Intrusive PCE methods converge significantly faster than the non-intrusive PCE and Monte Carlo[103].

Applications of intrusive PCE in FDTD are presented in refs. 105,106. Fabrication tolerances for the metallic parts of microwave circuits were taken into account[105], and FDTD was formulated on a statistically deformable, generalized curvilinear computational mesh (Fig. 2b).

Brillouin diagrams for periodic structures

Periodic structures are common in electromagnetic problems. Fields in periodic structures are subject to the Floquet theorem[107], which determines the relation between field components one lattice period apart. This relation is translated to PBCs enabling infinite periodic structures to be modelled via the simulation of a single unit cell, terminated in PBCs, as shown in Fig. 3a.

PBC algorithms for FDTD models may be divided into two groups: direct field methods, which use Maxwell's equations and their standard FDTD implementation, and field transformation methods that introduce auxiliary fields and update equations for these fields. A thorough review is provided in ref. 108.

FDTD models equipped with PBCs have extracted Brillouin band diagrams — angular frequency ω versus wavevector **k** — of periodic structures[109–112]; band diagrams for microwave[113] and optical[114] metamaterials; scattering from periodic structures, such as frequency selective surfaces[115,116]; and analysis of infinite phased arrays[117,118]. As an example, a 2D lattice of alumina cylinders modelled as one unit cell in an FDTD grid is shown in Fig. 3a. Figure 3b shows the corresponding FDTD-calculated band diagram for the geometry of Fig. 3a.

S-parameters for microwave circuits

Scattering parameters (*S*-parameters) are the most common network parameters to describe the performance of microwave circuits and devices in the frequency domain. Figure 3c shows a split ring resonator or strip wire structure[119]. In Fig. 3d, the results of an FDTD simulation are presented, with the structure placed in a computational domain terminated in PMCs in the lateral direction, PECs in the vertical direction and PMLs in the longitudinal direction. The normal incidence of a vertically polarized plane wave is simulated onto an infinite array of split ring resonator/strip wires. FDTD is used to determine the reflection coefficient S_{11} and transmission coefficient S_{21}. The source is a modulated Gaussian pulse $g(t) = \exp(-(t-t_0)^2/T_s^2)\sin(2\pi f_c t)$, in which f_c = 14 GHz, $t_0 = 3T_s$ and T_s = 7.5 ps to provide sufficient bandwidth to extract the scattering parameters in the frequency range between 0 and 22 GHz. The incident and total electric fields are sampled on the probe plane in front of the unit cell. The reflected electric field is obtained by subtracting the total field from the incident. The total transmitted electric field is sampled on a similar probe plane behind the unit cell. The waveforms of the incident, reflected and transmitted fields are Fourier-transformed. Then, the Fourier transform of the reflected and transmitted electric fields is divided by the Fourier transform of the incident field to compute S_{11} and S_{21}, respectively. The magnitude of these coefficients is shown in Fig. 3d.

Applications

This section highlights some technological areas where the FDTD method has provided important results and insights.

Biomedical

FDTD is a valuable tool for simulation and optimization in bioimaging, biophotonics, bioelectronics and biosensors. It is versatile at modelling different imaging modality setups, tissue structures and physical properties. The FDTD method has been used to validate and improve optical coherence tomography (OCT), partial wave spectroscopy (PWS), surface-enhanced Raman scattering and MRI. For example, the FDTD method was used to design a silicon-based metalens for the sample arm of a conventional ultrahigh resolution OCT[120], achieving a 30-fold increase in depth of focus compared with traditional objectives with similar resolution. By determining the underlying relationship between subdiffractional information in OCT images and biological sample statistics,[121] the high-resolution ultrastructure of biological features can be investigated using a traditional diffraction-limited setup. The FDTD method had a significant role in validating interferometric spectroscopy for optical statistical nanosensing, specifically the quantification of subdiffractional refractive-index variations in biological media, which led to the development of PWS microscopy[122], as shown in Fig. 4a. PWS has been applied to measure genome structures at length scales below the resolution of conventional microscopy[123]. An FDTD-aided design of nanoparticle layers was used[124] as a surface-enhanced Raman scattering substrate to enhance small molecule detection. To achieve simultaneous improvement in transmission efficiency and reception sensitivity in MRI, FDTD was used[125] to design a band-pass birdcage radio frequency coil by combining a multichannel wireless radio frequency element with a high permittivity material.

Beyond bioimaging, the FDTD method has been used to study the direct interaction of electromagnetic fields with biological materials for the safety evaluation of electromagnetic absorption[126,127] and numerical dosimetry[128], as has been shown in Fig. 4b. It has also been used to investigate cell behaviours and disease biomarkers related to retinal rods[129] (Fig. 4c), cervical cells[130], mitochondrial aggregation[131] and cancer cells[132]. The design of wearable devices[133] and antennas[134],

miniaturized biosensors[36,135], nanolenses[37] and microwave thermal ablation technologies[127] has been enhanced with FDTD.

Geophysics

Vegetation, rocks, soil, snow and the ionosphere have complex constitutive properties often exhibiting inhomogeneity, dispersion and anisotropy. Because the FDTD method is versatile at handling such conditions, it has been applied to geophysical problems across a range of frequencies and spatial scales.

FDTD applications in geophysics include simulation of ground-penetrating radar for the detection and localization of objects buried underground or geological anomalies[136], borehole sensors in geophysical exploration[137], remote sensing of ionosphere anomalies and hydrocarbon deposits[68], hypothesized electromagnetic earthquake precursors[68], space weather hazards[138], long-range radio communications[139–144], propagation from lightning[145] and high-frequency propagation through the magnetized ionosphere[146,147].

Figure 5a shows an efficient strategy for modelling electromagnetic wave propagation over long propagation paths in the Earth–ionosphere waveguide by taking advantage of the symmetry and signal movement. Figure 5b provides results for an 8-Mm radio path using the model of Fig. 5a. For some propagation geometries and ranges, a fully 3D FDTD model may be required to accurately predict the propagation characteristics[144].

Both 3D localized and global models of the Earth–ionosphere waveguide have been generated[68]. Figure 5c provides example electromagnetic propagation results for a pulse propagating globally around the Earth under ionospheric conditions predicted by the whole atmosphere community climate model with thermosphere and ionosphere extension.

Metamaterials

Artificial dielectrics with properties beyond those encountered in natural media — referred to as metamaterials — have led to the discovery of novel structures that support unconventional wave phenomena. Examples include negative refraction and inverted Doppler shift, along with related applications such as planar, sub-wavelength focusing lenses, electromagnetic cloaks and continuously scanning leaky-wave antennas. The transient behaviour of metamaterials may be naturally resolved by FDTD simulations. For example, the causal evolution of negative refraction was initially disputed and was verified in several FDTD papers, which illustrated the transient development of negatively refracted wavefronts at the interface between a positive-index and negative-index medium[148–150].

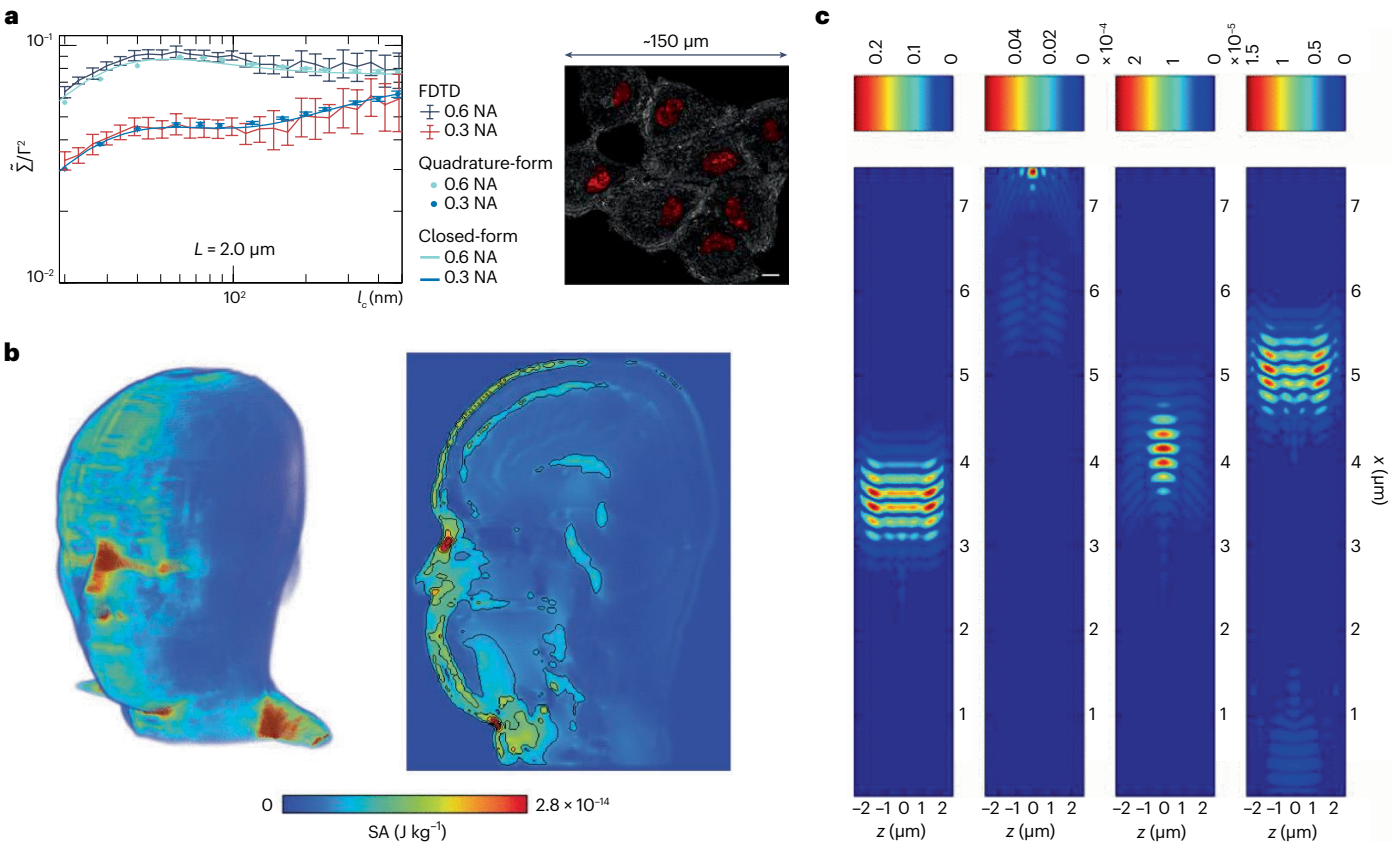

Fig. 4 | The finite-difference time-domain method applied to the biomedical field. a, Left: theoretical derivation of the partial wave spectroscopy imaging modality, supported by the finite-difference time-domain (FDTD) method. Right: experimental partial wave spectroscopy image (scale bar, 20 μm), revealing chromatin activities in live cells. **b**, Distribution of specific energy absorption (SA) on the surface (left) and inside the human head (right) of an FDTD-based numerical dosimetry study. **c**, Propagation of $|E_y|$ inside the outer segment of the photoreceptor cell for four different snapshots in time calculated by the FDTD method. NA, numerical aperture. Part **a** reprinted with permission from ref. 122, APS, and ref. 123, AAAS. Part **b** reprinted with permission from ref. 128, IEEE. Part **c** reprinted with permission from ref. 129, IEEE.

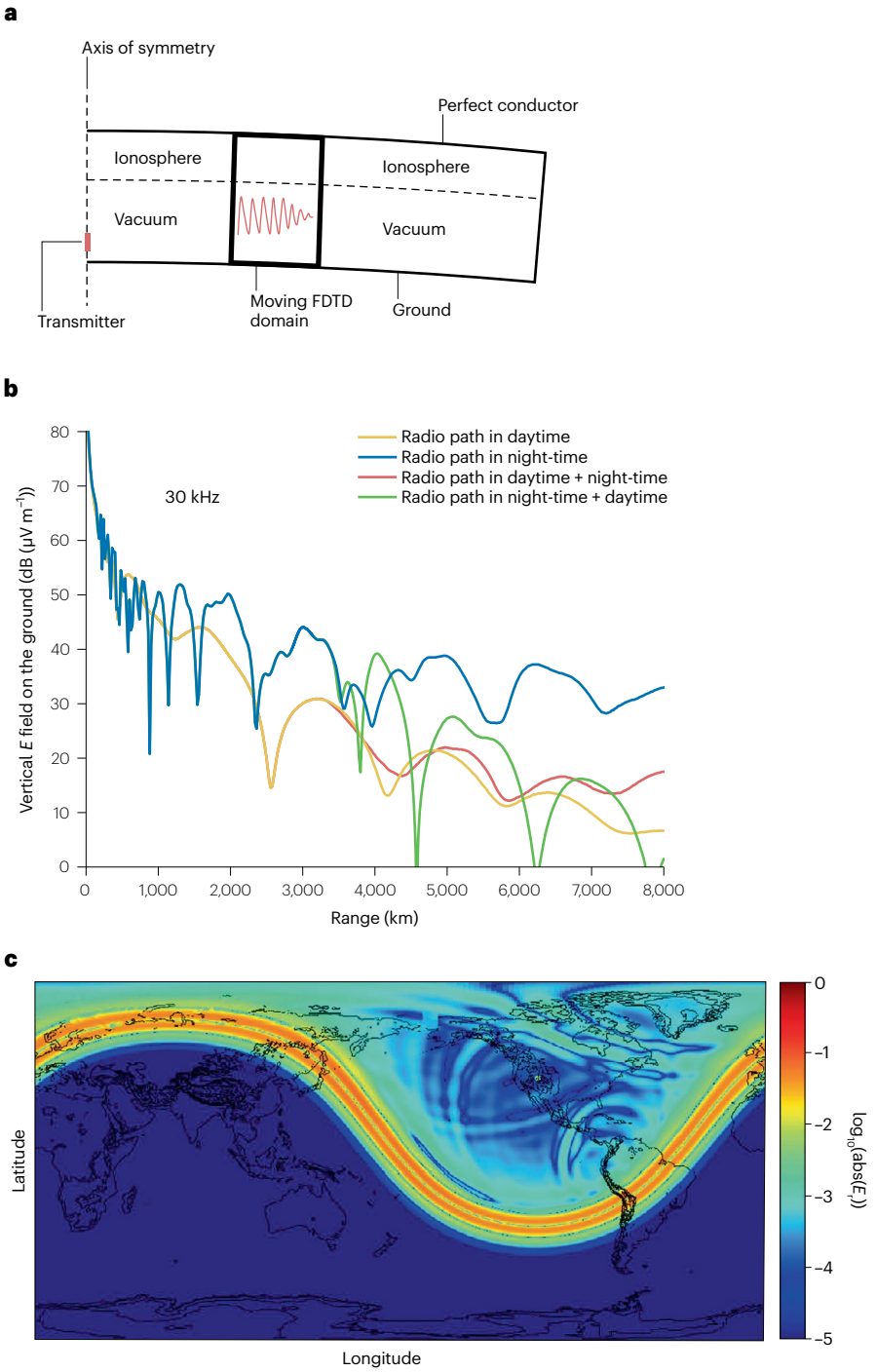

Fig. 5 | The finite-difference time-domain method applied to electromagnetic propagation in the Earth–ionosphere waveguide. a, An efficient axially symmetric (2.5-D) finite-difference time-domain (FDTD) computational domain model. **b**, Electromagnetic propagation results calculated by the model of part **a** over an 8-Mm radio path originating from a ground-level 1-kW vertical transmitter operating at 30 kHz. Ground ($\varepsilon_r = 15, \sigma = 0.01$ ohm m) is assumed from the transmitter to a distance of 2 Mm and seawater ($\varepsilon_r = 80, \sigma = 4$ ohm m) is assumed thereafter. The geomagnetic field is oriented 45° from the ground and 45° from the plane of propagation. The vertical electric field strength is plotted for typical day ($\beta = 0.3$, $h' = 72$ km) and night ($\beta = 0.5$, $h' = 87$ km) exponential ionospheres over the whole path. For the day + night case, day is assumed up to 3 Mm and night beyond 4 Mm, with a continuous terminator from 3 Mm to 4 Mm. The reverse is assumed for the night + day scenario. Compared with the uniform ionosphere scenarios, the effect of the terminator on the signal is visible from about 3.5 Mm from the transmitter. The calculations were performed using horizontal and vertical grid cell dimensions of 1 km and 1.33 km, respectively, and time-step increment of 2.53 ms. **c**, Example of electromagnetic propagation results from a 3D global FDTD model[69]. A horizontal plane of radial electric field components (E_r) sampled just above the surface of the Earth at 3.75 ms for a 300-Hz pulse occurring from Salt Lake City, UT, USA at 10 pm UTC. The 3D ionospheric conditions are defined by the whole atmosphere community climate model with thermosphere and ionosphere extension.

Figure 6 provides an example of FDTD simulation results for metamaterials. As shown in the inset of Fig. 6, a negative index lens is modelled consisting of a dispersive slab in between two semi-infinite free space regions[151]. Figure 6 shows the transient evolution of the electric field on the left and right interfaces of the lens at the design frequency (15.98 GHz). As predicted by the theory of the perfect lens[152], the electric field on the exit face is larger than the electric field at the input owing to growing evanescent waves within the negative index slab.

Optics and plasmonics

The FDTD method is one of the main workhorse simulation techniques in optics[153]. FDTD is a flexible tool for accurately modelling optical devices with fine geometrical details and a high degree of field

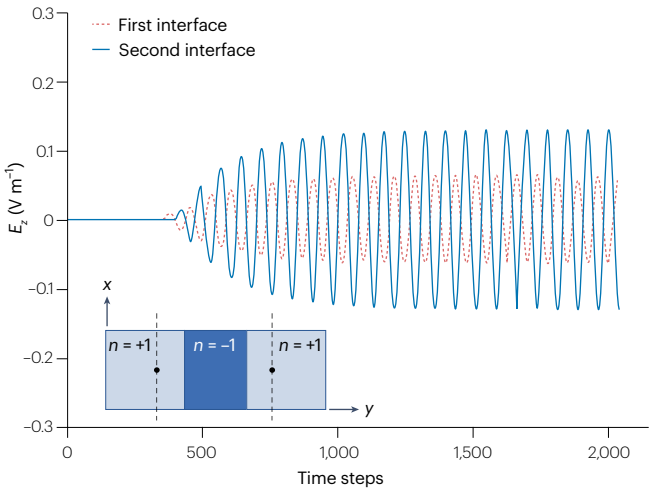

Fig. 6 | The finite-difference time-domain method applied to a metamaterial: a negative index lens. Electric field as a function of time at the first and second interfaces of the negative index lens ($n = -1 + j0.01$), with geometry shown in the inset. The source and image planes are indicated with dashed lines. The negative index medium is implemented as a Drude dispersive medium. Adapted with permission from ref. 151, IEEE.

confinement. Owing to this flexibility, it has been used to make new discoveries, such as the existence of the photonic nanojet[154,155]. Other examples include diffractive optical elements[156], photonic bandgap structures[157], grating couplers[158], photonic crystal waveguides[159], waveguide bends[160] and ring-resonator devices[161].

The FDTD method is also suitable for simulating plasmonic structures that explore surface plasmons — collective electron excitations — at metal–dielectric interfaces[162–164], or for confining and manipulating light below the diffraction limit. For example, the FDTD method has been applied to the design of a plasmonic super-directive antenna[165]. As another example, Fig. 7 shows cross-sectional snapshots of a 3D FDTD simulation of an electric field guided at $\lambda = 516.67$ nm along a T-shaped chain of gold nanospheres with 25-nm diameter and 75-nm intercentre spacing. The FDTD mesh is terminated by a PML and is composed of 448 × 544 × 256 cells with cubic grid cells of size 1.5625 nm. As seen in Fig. 7, the coupling of plasmon resonances between adjacent nanospheres produces a guided field with deep-sub-wavelength confinement along the chain.

Quantum FDTD

There are two fundamental classes of subatomic particles: fermions — electrons, protons and neutrons — which make up matter; and bosons — photons, gluons and bosons — which carry forces. Density-functional theory[166–169] is an effective quantum-mechanical computational method for solving the approximate electronic structures of many-body, fermionic systems. It is particularly useful for designing (artificial) materials in solid-state physics. However, single photons, bosons, are ideal for carrying quantum information as they barely interact with the environment or with each other.

Superposition and entanglement are the two major factors in developing quantum information science technology. First, to correctly model and design quantum electromagnetic systems, the quantization of classical electromagnetic systems is needed. The second quantization method is the standard quantization approach[170–174]. The main idea is to find eigenmodes of Helmholtz or vector wave equations, which may be viewed as electromagnetic uncoupled harmonic oscillators.

Finding numerical eigenmodes may be computationally expensive when photons carry broadband quantum information. In this case, the FDTD method is advantageous. In recent work[175], the original second quantization formulation was extended to use the FDTD method. By applying the unitary transformation to mode-ladder operators, electric field operators are rewritten in terms of the convolution between a new propagator and coordinate-ladder operators. The new propagator may be found using typical FDTD simulations. Once the new propagator is found, the expectation value of arbitrary observables — such as coincidence count — with respect to an initial quantum state are found. Note that initial quantum states are solutions to the quantum state equation or Schrödinger equation, describing the initial state of a system[170,171,174–177]. The Hamiltonian is time-independent in this system. See, for example, ref. 175, which provides a 1D FDTD solution for the new propagator.

Figure 8 depicts simulation results of the Hong–Ou–Mandel (HOM) effect, a well-known quantum physics phenomenon to measure the indistinguishability of two input photons. If the photons are indistinguishable, the destructive interference between them in a 50/50 beam splitter produces a bunching effect, causing the output photons to be measured at the same output port randomly. The degree of indistinguishability is often quantified using the second-order correlation function or normalized coincidence of two photodetections at both output ports, represented by $g^{(2)}$, which encodes the intensity fluctuations. A value of $g^{(2)}$ below 0.5 indicates the quantum nature of electromagnetic fields. The HOM effect has been successfully modelled using the numerical mode decomposition framework[175]. The aim is to achieve the same HOM effect using the quantum FDTD scheme. As shown in Fig. 8, both results are in strong agreement, showing the validity of the quantum FDTD method.

Multiphysics modelling

The FDTD method has been coupled to several other solvers to model multiphysics phenomena. For example, electromagnetic–thermal coupling was shown in ref. 178, in which the FDTD method was used to determine the steady-state field distribution on the conducting parts of a microelectromechanical switch. Additionally, FDTD algorithms have been developed for the Schrödinger equation to model quantum phenomena and for the coupled system of Maxwell and Schrödinger equations for coupled electromagnetic–quantum effects. Furthermore, the FDTD method has been coupled to charge transport models to replace quasistatic models for semiconductor devices, such as microwave field effect transistors and power amplifiers[179,180]. The FDTD-computed electromagnetic fields are linked to hydrodynamic equations — current continuity, energy and momentum conservation equations — that were used to determine the charge distribution and current density in the device. As a last example, FDTD time stepping may be linked to the Simulation Program with Integrated Circuit Emphasis (SPICE) models of linear and nonlinear electronic circuits and systems[181,182] to model wave–circuit interactions in structures such as active antennas, diode-reconfigurable microwave components and high-speed interconnects.

FDTD is readily coupled to ordinary and partial differential equation solvers in the time domain, facilitating modelling of dynamic phenomena. For example, coupled electromagnetic-circuit

simulations may be run by linking FDTD to SPICE-type solvers and using the same time step to synchronously model wave–circuit interactions[181,182]. Similarly, FDTD may be coupled to heat equation solvers to model the transient evolution of temperature in lossy media in the presence of electromagnetic fields. Such simulations can include temperature-dependent media, whose constitutive properties may be adjusted as the temperature changes, taking advantage of the dynamic nature of FDTD modelling. Finally, multiphysics phenomena can also involve extreme multiscale modelling. A recent example is the quantum–electromagnetic modelling of nanowires, in which an alternating-direction hybrid implicit–explicit FDTD technique was used to circumvent the extreme stability limit of conventional FDTD imposed by the presence of nanowires in the computational domain[183].

Reproducibility and data deposition

Reproducing FDTD data using alternative implementations of the FDTD algorithm requires information about the geometry of the problem — including specification of sources, material and boundary conditions — and information on the parameters of the FDTD algorithm, such as grid cell size and time step. If all simulation parameters are aligned, minor discrepancies between the results, for instance, deviations in the computed time-domain waveforms, may be attributed to differences in the absorbing boundary conditions, including implementation of PMLs, or differences in the treatment of material boundaries using staircasing, subcell or other techniques.

Discrepancies between FDTD simulated and measured data may result from minor discrepancies between material parameters owing to random fluctuations of the dielectric permittivity and conductivity of materials, or discrepancies between the physical and simulated geometry owing to discretization, for instance, staircasing of slanted boundaries.

FDTD results may be reproduced by other simulation methods, both differential and integral equation-based. Comparison between such data sets must consider the different ways each method accumulates numerical errors. As a result, comparisons cannot rely on aligning the simulation parameters of each method. However, comparisons may be made between the convergent results of FDTD and other methods, determined by varying the simulation parameters, such as cell size.

No data repository specific for FDTD results exists at present. However, many university and journal-based repositories provide results from individual research laboratories and publications. Furthermore, many commercial software companies offer data sets that may be used as inputs to FDTD models.

Limitations and optimizations

To avoid poor FDTD modelling results and unexpected outcomes, it is important to understand the limitations of the FDTD method. Several limitations — numerical dispersion, staircasing error and stability limit — were discussed in the preceding sections and are not considered again here. Rather, some additional limitations of the FDTD algorithm are briefly discussed, along with workarounds and optimizations.

Speeding up FDTD simulations

The maximum time-step increment for the conventional FDTD method is limiting. Alongside unconditionally stable FDTD methods, other workarounds are available to improve the performance of the FDTD method for long simulations. For example, in lossy media at sufficiently low frequencies, the conduction current may be stronger than the displacement current by several orders of magnitude. It is possible to scale up the permittivity and time-step increment Δt while minimally affecting the accuracy of the results[184]. Other types of parameter scaling may also be used[185].

Other options for speeding up an FDTD simulation include relaxing the stability limit by applying a spatial filter to the simulated field components to suppress unstable spatial harmonics[186]; applying signal-processing techniques to extrapolate the results from a short FDTD simulation to later time points[187,188] and approximating the continuation of geometries via PBCs. The final approach was used to simulate high-frequency electromagnetic propagation through the ionosphere[189].

Additive errors from numerical dispersion

In addition to phase error, numerical dispersion effects may also introduce additive errors into FDTD-calculated data. Numerical dispersion effects establish a dependence of the numerical wave impedance on the FDTD grid cell size. This dependence causes an impedance mismatch at the subgridding interfaces where the cell size abruptly changes. Such impedance mismatches produce spurious reflections, which are additive errors. The application of spatial filters to the modified FDTD update equations at the subgridding interfaces may mitigate additive errors[190].

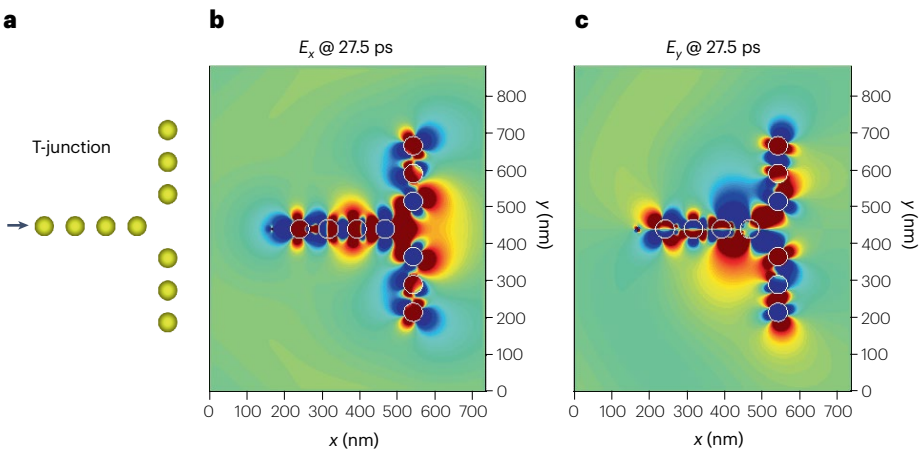

Fig. 7 | The finite-difference time-domain method applied to plasmonics. a, A diagram of a T-junction chain of gold nanospheres. **b**,**c**, Finite-difference time-domain cross-sectional snapshots of the amplitude of the electric field components E_x (panel **b**) and E_y (panel **c**) along the T-junction chain of gold nanospheres. The chain is excited by an x-oriented dipole to the left (indicated by the arrow), with wavelength $\lambda = 516.67$ nm. The nanospheres have 25-nm diameter and 75-nm intercentre spacing. The gold permittivity is represented by a Drude model with a relaxation time $\tau = 4$ fs and bulk plasmon frequency $\omega = 6.79 \times 10^{15}$ rad s^{-1}. Coupling of the plasmon resonances between adjacent nanospheres produces the guided field propagation with deep-sub-wavelength confinement.

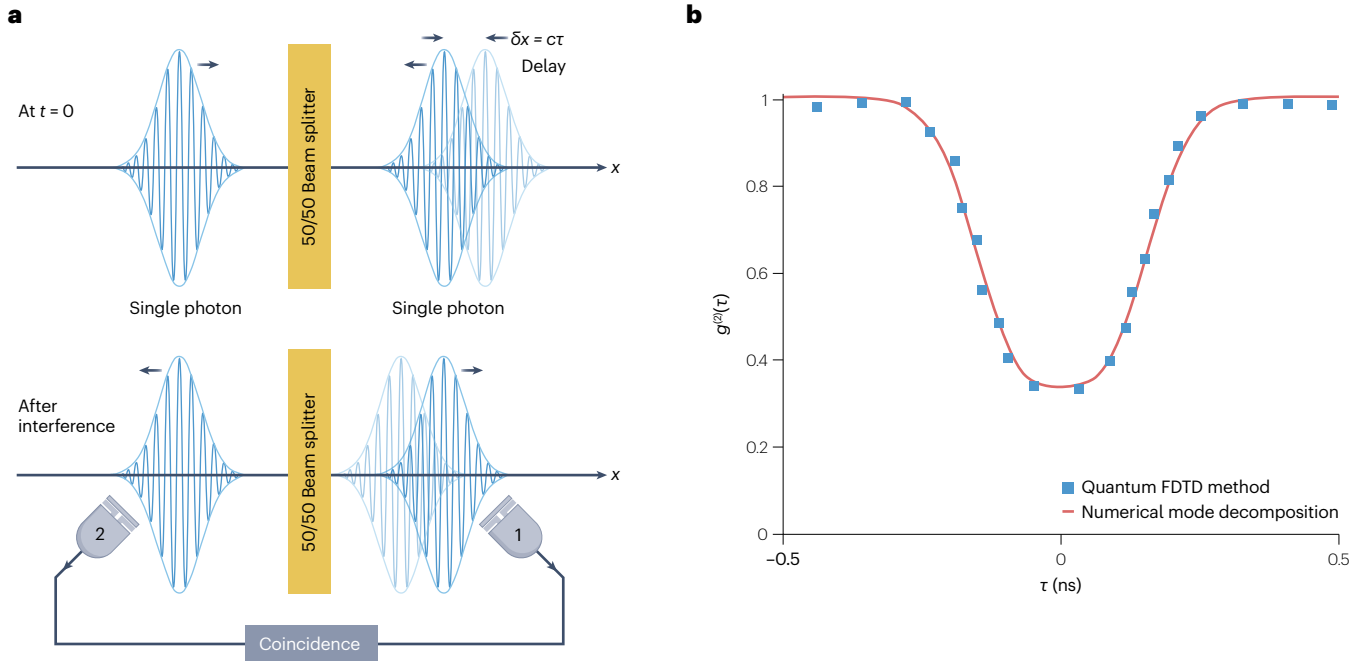

Fig. 8 | Results from a quantum finite-difference time-domain model. a, Schematic of the simulated quantum beam splitter to observe the Hong–Ou–Mandel effect. **b**, The Hong–Ou–Mandel effects are numerically evaluated by using numerical canonical quantization (solid line) and Q-finite-difference time-domain (FDTD) method (square markers).

Source implementation artefacts

FDTD is a charge-conserving algorithm. As a result, current source distributions must either be divergence-free or have no direct current offset to avoid charge deposition on the FDTD grid nodes. Such node-deposited charges are stationary and equivalent to infinitely massive-charged particles that produce spurious static fields[191].

A sudden initiation of a source at $t = 0$ may lead to the excitation of high-frequency field transients that are poorly resolved in the FDTD grid that alter the results. Smoothing ramp functions may be applied to the early source signals to reduce such high-frequency components[184].

Unconditional instabilities

Special care must be taken when implementing nontrivial modifications to the FDTD method, such as adding subgrids or using non-orthogonal FDTD algorithms, to avoid unconditional instabilities[192–194]. Such instabilities may arise from subtle inconsistencies in the spatial discretization. This may lead to a violation of the mathematical properties (div curl = 0 or curl grad = 0) or physical principles, such as positive definiteness of the electromagnetic energy density or reciprocity, in the discrete setting. Discrete exterior calculus tools are useful for avoiding inconsistencies during the spatial discretization process[195–197].

Outlook

This section highlights current challenges and opportunities for the FDTD method, as well as ongoing and future priorities and applications.

Challenges

Despite the rapid growth and widespread use of the FDTD method, challenges remain. For example, the FDTD method is limited by numerical dispersion and stability. Large-scale problems are generally solvable by the FDTD method only on high-performance computing platforms. Unlike integral equation methods, which connect source and observation points via Green's functions, the FDTD method requires global discretization of the entire computational domain. To accelerate the modelling of thin sheets, including metasurfaces, stable FDTD implementations of surface impedance and generalized sheet transition conditions are needed. PMLs add to the computational cost of a 3D simulation. Boundary integral approaches destroy the matrix-free nature of FDTD. A challenge remains to find a thinner, but still effective, absorbing boundary condition while preserving the matrix-free nature of FDTD. Finally, subgridding approaches have been developed but more stable algorithms that permit larger time-stepping increments are needed.

Opportunities for FDTD

Although there are challenges, there are also numerous opportunities for the FDTD method.

Scientific machine learning. Scientific machine learning is driven by three fundamental questions: how can training data sets be generated by sampling a set of model input parameters? How should efficient learning structures be chosen among the many existing and emerging forms of neural networks? And what types of objectives — field computation, scattering parameters, optimization and uncertainty quantification — should be targeted by developing such models? Each of these questions may be considered in the context of FDTD modelling.

Standard PINNs use automatic differentiation to compute any derivatives included in their loss functions. Alternatively, decades of FDTD research may be applied to approximate these derivatives on

uniform, non-uniform or subgridded FDTD meshes. A recent study has shown that such an approach results in PINNs that may use time steps beyond the CFL constraint for the corresponding FDTD grid[98]. This is a promising direction for further research.

FDTD as a design optimization tool. The FDTD method has three distinct advantages as a design tool: accuracy, versatility and the ability to provide broadband characterization of geometries in a single simulation. Computational costs may be overcome by using efficient techniques to compute the output function derivatives with respect to the input parameters, such as the adjoint variable method[198]. Surrogate models can be developed via a reduced number of FDTD simulations[199]. Furthermore, high-performance computing resources and hardware acceleration can be used, as shown in a recent 3D simulation of a $100\lambda \times 100\lambda$ area metalens simulation in less than 5 min using hardware-accelerated FDTD[200].

Quantum FDTD prospects. Evolving from scientific proof-of-principle experiments, quantum technologies are poised to be distributed in chips on the basis of nano-optics technology, photonic integrated circuits and microwave engineering technology[201]. This is a crucial step towards scalable quantum systems. It also necessitates an effective full-wave physics numerical framework that can simulate the time evolution of quantum information carried by single or entangled photons in a complex environment. Extending the 1D quantum FDTD scheme into higher-dimensional space involving a lossy environment will be important to understand the full physics of quantum information propagation at the on-chip level. It will also benefit a range of other quantum technologies, such as quantum communications, quantum computing and quantum sensing.

Other novel approaches in development. Research developments include higher-order methods for high accuracy at coarse discretization rates, using concepts from FETD and the discontinuous Galerkin time-domain method[202]. The stable and robust hybridization of FDTD with other methods — such as the method of moments, the finite-element method, ray tracing and the vector parabolic equation method — continues to attract attention.

The FDTD method registers the complete history of pulses propagating through a computational domain, along with its multiple reflections from objects and discontinuities. However, the sharp edge of a microstrip structure may not be continuously illuminated by the initial and reflected pulses. Therefore, static mesh refinement is a suboptimal solution to the grid refinement problem. To overcome this, adaptive mesh refinement strategies based on the intelligent mesh regeneration and dynamic adaptivity during simulation time[203] may be used.

Attempts have been made to hybridize FDTD with other frequency-domain and time-domain numerical techniques. For example, ref. 204 hybridized FDTD with the method of moments to efficiently embed thin-wire antennas in an FDTD mesh without invoking thin-wire or subgridding techniques. In ref. 205, FDTD was combined with ray tracing to solve indoor wireless propagation problems. Ray tracing modelled propagation over electrically large distances, whereas FDTD was applied to compute the interaction of wireless signals with walls and corners. Generally, hybrid methods follow a similar pattern of exploiting the versatility of FDTD, while improving its efficiency for a particular class of problems by using a different method. These hybridizations take advantage of the fundamental connections between numerical techniques[206].

Future priorities and applications

Priorities for FDTD research include exploiting new high-performance computing resources and hardware to expand FDTD to larger-scale problems; integrating machine-learning algorithms in FDTD computations; developing FDTD algorithms on quantum computers; using the FDTD method for inverse problems and design optimization by integrating with other methods and topology optimizations; developing stable, highly-accurate space–time subgrids for extreme multiscale problems; and exploring multiphysics FDTD algorithms, including quantum, chemical and mechanical effects.

The impact of the FDTD method is likely to see continual growth for a diverse range of applications. This includes inverse designs and optimizations of meta-structures in microwaves and optics; modelling and optimization of time-varying metasurfaces; and analysis of wireless communication links, such as radiation exposure studies. Another area where growth is expected is in simulating biological phenomena, including multiphysics interactions in molecular communications, for example, protein folding stimulated by terahertz waves and therapeutic applications of electromagnetic fields. One last example is modelling extreme multiscale structures, including quantum effects.

Published online: 05 October 2023

References

1. Maxwell, J. C. VIII. A dynamical theory of the electromagnetic field. *Philos. Trans. R. Soc. Lond.* **155**, 459–512 (1865).
2. Chew, W. C. et al. Quantum Maxwell's equations made simple: employing scalar and vector potential formulation. *IEEE Antennas Propag. Mag.* **63**, 14–26 (2020).
3. Kong, J. A. *Electromagnetic Wave Theory* (Wiley, 1990).
4. Balanis, C. A. *Advanced Engineering Electromagnetics* 2nd edn (Wiley, 2012).
5. Yee, K. Numerical solution of initial boundary value problems involving Maxwell's equations in isotropic media. *IEEE Trans. Antennas Propag.* **14**, 302–307 (1966).
Paper in which Yee introduced the FDTD method.
6. Courant, R., Friedrichs, K. & Lewy, H. Über die partiellen differenzengleichungen der mathematischen Physik. *Math. Ann.* **100**, 32–74 (1928).
7. Taflove, A. & Hagness, S. C. *Computational Electromagnetics: The Finite-Difference Time-Domain Method* 3rd edn (Artech House, Inc., 2005).
A thorough overview of many key algorithms and applications of the method.
8. Tan, T. & Potter, M. FDTD discrete planewave (FDTD-DPW) formulation for a perfectly matched source in TFSF simulations. *IEEE Trans. Antennas Propag.* **58**, 2641–2648 (2010).
9. Harms, P., Mittra, R. & Ko, W. Implementation of the periodic boundary condition in the finite-difference time-domain algorithm for FSS structures. *IEEE Trans. Antennas Propag.* **42**, 1317–1324 (1994).
10. Kesler, M. P., Maloney, J. G., Shirley, B. L. & Smith, G. S. Antenna design with the use of photonic band-gap materials as all-dielectric planar reflectors. *Microw. Opt. Technol. Lett.* **11**, 169–174 (1996).
11. Smith, D. R., Burns, S., Simpson, J. J. & Ferrone, S. M. FDTD modeling of scattered ultra-low frequency electromagnetic waves from objects submerged in the ocean. *IEEE Trans. Antennas Propag.* **67**, 2534–2541 (2019).
12. Oh, K. S. & Schutt-Aine, J. E. An efficient implementation of surface impedance boundary conditions for the finite-difference time-domain method. *IEEE Trans. Antennas Propag.* **43**, 660–666 (1995).
13. Beggs, J. H., Luebbers, R. J., Yee, K. S. & Kunz, K. S. Finite-difference time-domain implementation of surface impedance boundary conditions. *IEEE Trans. Antennas Propag.* **40**, 49–56 (1992).
14. Berenger, J.-P. A perfectly matched layer for the absorption of electromagnetic waves. *J. Comput. Phys.* **114**, 185–200 (1994).
15. Katz, D. S., Thiele, E. T. & Taflove, A. Validation and extension to three dimensions of the Berenger PML absorbing boundary condition for FDTD meshes. *IEEE Microw. Guided Wave Lett.* **4**, 268–270 (1994).
16. Chew, W. C. & Weedon, W. H. A 3D perfectly matched medium from modified Maxwell's equations with stretched coordinates. *Microw. Opt. Technol. Lett.* **7**, 599–604 (1994).
17. Teixeira, F. L. & Chew, W. C. Complex space approach to perfectly matched layers: a review and some new developments. *Int. J. Numer. Model. Electron. Netw. Devices Fields* **13**, 441–455 (2000).
Describes the PML concept and its various extensions with an emphasis on the complex coordinate mapping approach.
18. Kuzuoglu, M. & Mittra, R. Frequency dependence of the constitutive parameters of causal perfectly matched anisotropic absorbers. *IEEE Microw. Guided Wave Lett.* **6**, 447–449 (1996).

19. Teixeira, F. L. & Chew, W. C. Differential forms, metrics, and the reflectionless absorption of electromagnetic waves. *J. Electromagn. Waves Appl.* **13**, 665–686 (1999).
20. Sacks, Z. S., Kingsland, D. M., Lee, R. & Lee, J.-F. A perfectly matched anisotropic absorber for use as an absorbing boundary condition. *IEEE Trans. Antennas Propag.* **43**, 1460–1463 (1995).
21. Roden, J. A. & Gedney, S. D. Convolution PML (CPML): an efficient FDTD implementation of the CFS–PML for arbitrary media. *Microw. Opt. Technol. Lett.* **27**, 334–339 (2000).
22. Moreno, E. et al. Implementation of open boundary problems in photo-conductive antennas by using convolutional perfectly matched layers. *IEEE Trans. Antennas Propag.* **64**, 4919–4922 (2016).
23. Wang, J.-F., Li, G. & Chen, Z. Convolutional implementation and analysis of the CFS-PML ABC for the FDTD method based on wave equation. *IEEE Microw. Wirel. Compon. Lett.* **32**, 811–814 (2022).
24. Teixeira, F. L. Time-domain finite-difference and finite-element methods for Maxwell equations in complex media. *IEEE Trans. Antennas Propag.* **56**, 2150–2166 (2008).
Provides a thorough review of the FDTD algorithm applied to complex media.
25. Shibayama, J., Suzuki, K., Yamauchi, J. & Nakano, H. Trapezoidal recursive convolution-based FDTD method for arbitrary-shaped dispersive materials. *Electron. Lett.* **54**, 1429–1430 (2018).
26. Okoniewski, M., Mrozowski, M. & Stuchly, M. A. Computationally efficient algorithms for multi-term dielectric dispersion in FDTD. in *IEEE Antennas and Propagation Society International Symposium 1997* 364–367 (IEEE, 1997).
27. Pereda, J. A., Vielva, L. A., Solano, M. A., Vegas, A. & Prieto, A. FDTD analysis of magnetized ferrites: application to the calculation of dispersion characteristics of ferrite-loaded waveguides. *IEEE Trans. Microw. Theory Tech.* **43**, 350–357 (1995).
28. Okoniewski, M. & Okoniewska, E. FDTD analysis of magnetized ferrites: a more efficient algorithm. *IEEE Microw. Guided Wave Lett.* **4**, 169–171 (1994).
29. Yu, Y., Niu, J. & Simpson, J. J. A 3-D global earth–ionosphere FDTD model including an anisotropic magnetized plasma ionosphere. *IEEE Trans. Antennas Propag.* **60**, 3246–3256 (2012).
30. Ha, S.-G., Cho, J., Choi, J., Kim, H. & Jung, K.-Y. FDTD dispersive modeling of human tissues based on quadratic complex rational function. *IEEE Trans. Antennas Propag.* **61**, 996–999 (2013).
31. Choi, H., Baek, J.-W. & Jung, K.-Y. Comprehensive study on numerical aspects of modified Lorentz model-based dispersive FDTD formulations. *IEEE Trans. Antennas Propag.* **67**, 7643–7648 (2019).
32. Sullivan, D. M. Frequency-dependent FDTD methods using Z transforms. *IEEE Trans. Antennas Propag.* **40**, 1223–1230 (1992).
33. Kosmas, P., Rappaport, C. M. & Bishop, E. Modeling with the FDTD method for breast cancer detection. *IEEE Trans. Microw. Theory Tech.* **52**, 1890–1897 (2004).
34. Kast, M. J. & Elsherbeni, A. Z. Integration of nonlinear circuit elements into FDTD method formulation. in *Advances in Time-Domain Computational Electromagnetic Methods* (ed. Rodolfo, A.) 1–31 (SciTech Publishing, 2022).
35. Holland, R. THREDS: a finite-difference time-domain EMP code in 3d spherical coordinates. *IEEE Trans. Nucl. Sci.* **30**, 4592–4595 (1983).
36. Said, F. A. et al. FDTD analysis of structured metallic nanohole films for LSPR-based biosensor. in *IEEE Regional Symposium on Micro and Nanoelectronics* (*RSM*) (IEEE, 2015).
37. Mudanyali, O. et al. Wide-field optical detection of nanoparticles using on-chip microscopy and self-assembled nanolenses. *Nat. Photon.* **7**, 247–254 (2013).
38. Joseph, R. M. & Taflove, A. FDTD Maxwell's equations models for nonlinear electrodynamics and optics. *IEEE Trans. Antennas Propag.* **45**, 364–374 (1997).
39. Boyd, R. *Nonlinear Optics* 3rd edn (Academic Press, 2018).
40. Bhardwaj, S., Teixeira, F. L. & Volakis, J. L. Fast modeling of terahertz plasma-wave devices using unconditionally stable FDTD methods. *IEEE J. Multisc. Multiphys. Comput. Tech.* **3**, 29–36 (2018).
41. Biabani, S. & Foroutan, G. Self consistent multi-fluid FDTD simulations of a nanosecond high power microwave discharge in air. *Phys. Lett. A* **382**, 2720–2731 (2018).
42. Godfrey, B. B. & Vay, J.-L. Suppressing the numerical Cherenkov instability in FDTD PIC codes. *J. Comput. Phys.* **267**, 1–6 (2014).
43. Na, D.-Y. et al. Diagnosing numerical Cherenkov instabilities in relativistic plasma simulations based on general meshes. *J. Comput. Phys.* **402**, 108880 (2020).
44. Nicolaides, R. A method for complex geometries in finite-difference solutions of Maxwell's equations. *Comput. Math. Appl.* **48**, 1111–1119 (2004).
45. Lee, H. O. & Teixeira, F. L. Locally-conformal FDTD for anisotropic conductive interfaces. *IEEE Trans. Antennas Propag.* **58**, 3658–3665 (2010).
46. Zhao, Q. & Sarris, C. D. Generalized tensor FDTD method for sloped dispersive interfaces and thin sheets. *Opt. Express* **27**, 15812–15826 (2019).
47. Cabello, M. R. et al. A new efficient and stable 3D conformal FDTD. *IEEE Microw. Wirel. Compon. Lett.* **26**, 553–555 (2016).
48. Srisukh, Y., Nehrbass, J., Teixeira, F. L., Lee, J.-F. & Lee, R. An approach for automatic grid generation in three-dimensional FDTD simulations of complex geometries. *IEEE Antennas Propag. Mag.* **44**, 75–80 (2002).
Describes an automatic 3D FDTD grid generation for complex geometries.
49. Heinrich, W., Beilenhoff, K., Mezzanotte, P. & Roselli, L. Optimum mesh grading for finite-difference method. *IEEE Trans. Microw. Theory Tech.* **44**, 1569–1574 (1996).
50. Mezzanotte, P., Roselli, L., Huber, C., Zscheile, H. & Heinrich, W. On the accuracy of the finite-difference method using mesh grading. in *Proceedings of 1995 IEEE MTT-S International Microwave Symposium* Vol. 2, 781–784 (IEEE, 1995).
51. Maloney, J. G. & Smith, G. S. The efficient modeling of thin material sheets in the finite-difference time-domain (FDTD) method. *IEEE Trans. Antennas Propag.* **40**, 323–330 (1992).
52. Farjadpour, A. et al. Improving accuracy by subpixel smoothing in the finite-difference time domain. *Opt. Lett.* **31**, 2972–2974 (2006).
53. Nadobny, J., Sullivan, D., Wlodarczyk, W., Deuflhard, P. & Wust, P. A 3-D tensor FDTD-formulation for treatment of sloped interfaces in electrically inhomogeneous media. *IEEE Trans. Antennas Propag.* **51**, 1760–1770 (2003).
Introduces a tensor FDTD formulation for the treatment of non-rectangular boundaries crossing a Yee cell.
54. Karkkainen, M. K. Subcell FDTD modeling of electrically thin dispersive layers. *IEEE Trans. Microw. Theory Tech.* **51**, 1774–1780 (2003).
55. Zhao, Y. & Hao, Y. Finite-difference time-domain study of guided modes in nano-plasmonic waveguides. *IEEE Trans. Antennas Propag.* **55**, 3070–3077 (2007).
56. Chevalier, M. W., Luebbers, R. J. & Cable, V. P. FDTD local grid with material traverse. *IEEE Trans. Antennas Propag.* **45**, 411–421 (1997).
57. Kim, I. S. & Hoefer, W. J. R. A local mesh refinement algorithm for the time domain-finite difference method using Maxwell's curl equations. *IEEE Trans. Microw. Theory Tech.* **38**, 812–815 (1990).
58. Zivanovic, S. S., Yee, K. S. & Mei, K. K. A subgridding method for the time-domain finite-difference method to solve Maxwell's equations. *IEEE Trans. Microw. Theory Tech.* **39**, 471–479 (1991).
59. Okoniewski, M., Okoniewska, E. & Stuchly, M. A. Three-dimensional subgridding algorithm for FDTD. *IEEE Trans. Antennas Propag.* **45**, 422–429 (1997).
60. Kulas, L. & Mrozowski, M. Low-reflection subgridding. *IEEE Trans. Microw. Theory Tech.* **53**, 1587–1592 (2005).
61. Thoma, P. & Weiland, T. A consistent subgridding scheme for the finite difference time domain method. *Int. J. Numer. Model. Electron. Netw. Devices Fields* **9**, 359–374 (1996).
Presents consistent and provably stable formulations for FDTD subgridding.
62. Xiao, K., Pommerenke, D. J. & Drewniak, J. L. A three-dimensional FDTD subgridding algorithm with separated temporal and spatial interfaces and related stability analysis. *IEEE Trans. Antennas Propag.* **55**, 1981–1990 (2007).
Presents consistent and provably stable formulations for FDTD subgridding.
63. Berenger, J.-P. Origin of parasitic solutions with Holland and Simpson thin wires in the FDTD grid. *IEEE Trans. Electromagn. Compat.* **61**, 487–494 (2019).
Describes the origin of the parasitic solutions for the thin-wire formulation.
64. Holland, R. & Simpson, L. Finite-difference analysis of EMP coupling to thin struts and wires. *IEEE Trans. Electromagn. Compat.* **EMC-23**, 88–97 (1981).
65. Teixeira, F. L. & Chew, W. C. Finite-difference computation of transient electromagnetic waves for cylindrical geometries in complex media. *IEEE Trans. Geosci. Remote Sens.* **38**, 1530–1543 (2000).
66. Pérez-Ocón, F., Pozo, A. M., Jiménez, J. R. & Hita, E. Fast single-mode characterization of optical fiber by finite-difference time-domain method. *J. Lightwave Technol.* **24**, 3129 (2006).
67. Lee, H. O. & Teixeira, F. L. Cylindrical FDTD analysis of LWD tools through anisotropic dipping-layered earth media. *IEEE Trans. Geosci. Remote Sens.* **45**, 383–388 (2007).
68. Simpson, J. J. Current and future applications of 3-D global earth–ionosphere models based on the full-vector Maxwell's equations FDTD method. *Surv. Geophys.* **30**, 105–130 (2009).
Summarizes developments and applications of FDTD modelling of the Earth–ionosphere waveguide.
69. Simpson, J. J. & Taflove, A. Three-dimensional FDTD modeling of impulsive ELF propagation about the earth-sphere. *IEEE Trans. Antennas Propag.* **52**, 443–451 (2004).
70. Samimi, A. & Simpson, J. J. Parallelization of 3-D global FDTD earth–ionosphere waveguide models at resolutions on the order of ~1km and higher. *IEEE Antennas Wirel. Propag. Lett.* **15**, 1959–1962 (2016).
71. Lee, R. A note on mass lumping in the finite element time domain method. *IEEE Trans. Antennas Propag.* **54**, 760–762 (2006).
72. Teixeira, F. L. A summary review on 25 years of progress and future challenges in FDTD and FETD techniques. *Appl. Comput. Electromagn. Soc. J.* **25**, 1–14 (2022).
73. Rylander, T. & Bondeson, A. Stable FEM–FDTD hybrid method for Maxwell's equations. *Computer Phys. Commun.* **125**, 75–82 (2000).
74. Chilton, R. A. & Lee, R. Conservative and provably stable FDTD subgridding. *IEEE Trans. Antennas Propag.* **55**, 2537–2549 (2007).
75. Jung, K.-Y. & Teixeira, F. L. in *Advanced Time Domain Modeling for Electrical Engineering* (ed. Rodolfo, A.) 217–252 (SciTech Publishing, IET Press, 2022).
76. Tan, E. L. Fundamental schemes for efficient unconditionally stable implicit finite-difference time-domain methods. *IEEE Trans. Antennas Propag.* **56**, 170–177 (2008).
77. Shi, S.-B., Shao, W., Wei, X.-K., Yang, X.-S. & Wang, B.-Z. A new unconditionally stable FDTD method based on the Newmark-Beta algorithm. *IEEE Trans. Microw. Theory Tech.* **64**, 4082–4090 (2016).
78. Sun, G. & Trueman, C. W. Efficient implementations of the Crank–Nicolson scheme for the finite-difference time-domain method. *IEEE Trans. Microw. Theory Tech.* **54**, 2275–2284 (2006).
79. Moon, H., Teixeira, F. L., Kim, J. & Omelchenko, Y. A. Trade-offs for unconditional stability in the finite-element time-domain method. *IEEE Microw. Wirel. Compon. Lett.* **24**, 361–363 (2014).
80. Namiki, T. A new FDTD algorithm based on alternating-direction implicit method. *IEEE Trans. Microw. Theory Tech.* **47**, 2003–2007 (1999).

81. Zheng, F., Chen, Z. & Zhang, J. A finite-difference time-domain method without the Courant stability conditions. *IEEE Microw. Guided Wave Lett.* **9**, 441–443 (1999).
82. Yuan, C. & Chen, Z. D. On the modeling of conducting media with the unconditionally stable ADI-FDTD method. *IEEE Trans. Microw. Theory Tech.* **51**, 1929–1938 (2003).
83. Shibayama, J., Muraki, M., Yamauchi, J. & Nakano, H. Efficient implicit FDTD algorithm based on locally one-dimensional scheme. *Electron. Lett.* **41**, 1–2 (2005).
84. Nascimento, V. E., Borges, B.-H. V. & Teixeira, F. L. Split-field PML implementations for the unconditionally stable LOD-FDTD method. *IEEE Microw. Wirel. Compon. Lett.* **16**, 398–400 (2006).
85. Ong, C. et al. Speed it up. *IEEE Microw. Mag.* **11**, 70–78 (2010).
86. Shlager, K. L. & Schneider, J. B. Comparison of the dispersion properties of several low-dispersion finite-difference time-domain algorithms. *IEEE Trans. Antennas Propag.* **51**, 642–653 (2003).
87. Hadi, M. F. & Piket-May, M. A modified FDTD (2, 4) scheme for modeling electrically large structures with high-phase accuracy. *IEEE Trans. Antennas Propag.* **45**, 254–264 (1997).
88. Zhao, S. & Wei, G. W. High-order FDTD methods via derivative matching for Maxwell's equations with material interfaces. *J. Comput. Phys.* **200**, 60–103 (2004).
89. Law, Y.-M. & Nave, J.-C. High-order FDTD schemes for Maxwell's interface problems with discontinuous coefficients and complex interfaces based on the correction function method. *J. Sci. Comput.* https://doi.org/10.1007/s10915-022-01797-9 (2022).
90. Wang, S. & Teixeira, F. L. Lattice models for large-scale simulations of coherent wave scattering. *Phys. Rev. E* https://doi.org/10.1103/physreve.69.016701 (2004).
91. Finkelstein, B. & Kastner, R. A comprehensive new methodology for formulating FDTD schemes with controlled order of accuracy and dispersion. *IEEE Trans. Antennas Propag.* **56**, 3516–3525 (2008).
92. Zygiridis, T. T., Papadopoulos, A. D. & Kantartzis, N. V. Error-optimized finite-difference modeling of wave propagation problems with Lorentz material dispersion. *J. Comput. Phys.* **452**, 110916 (2022).
93. Karniadakis, G. E. et al. Physics-informed machine learning. *Nat. Rev. Phys.* **3**, 422–440 (2021).
94. Raissi, M., Perdikaris, P. & Karniadakis, G. E. Physics-informed neural networks: a deep learning framework for solving forward and inverse problems involving nonlinear partial differential equations. *J. Comput. Phys.* **378**, 686–707 (2019).
95. Sirignano, J. & Spiliopoulos, K. DGM: a deep learning algorithm for solving partial differential equations. *J. Comput. Phys.* **375**, 1339–1364 (2018).
96. E, W. & Yu, B. The deep Ritz method: a deep learning-based numerical algorithm for solving variational problems. *Commun. Math. Stat.* **6**, 1–12 (2018).
97. Zhang, P. et al. A Maxwell's equations based deep learning method for time domain electromagnetic simulations. *IEEE J. Multisc. Multiphys. Comput. Tech.* **6**, 35–40 (2021).
98. Qi, S. & Sarris, C. D. Electromagnetic-thermal analysis with FDTD and physics-informed neural networks. *IEEE J. Multisc. Multiphys. Comput. Tech.* **8**, 49–59 (2023).
99. Qi, S. & Sarris, C. D. Deep neural networks for rapid simulation of planar microwave circuits based on their layouts. *IEEE Trans. Microw. Theory Tech.* **70**, 4805–4815 (2022).
100. Folk, M., Heber, G., Koziol, Q., Pourmal, E. & Robinson, D. An overview of the HDF5 technology suite and its applications. in *AD '11 Proc. EDBT/ICDT 2011 Workshop on Array Databases* 36–47 (ACM, 2011).
101. Hastings, F. D., Schneider, J. B. & Broschat, S. L. A Monte-Carlo FDTD technique for rough surface scattering. *IEEE Trans. Antennas Propag.* **43**, 1183–1191 (1995).
102. Le Maître, O. & Knio, O. M. *Spectral Methods for Uncertainty Quantification: With Applications to Computational Fluid Dynamics* (Springer-Verlag, 2010).
103. Xiu, D. & Karniadakis, G. E. The Wiener–Askey polynomial chaos for stochastic differential equations. *SIAM J. Sci. Comput.* **24**, 619–644 (2002).
104. Xiu, D. *Numerical Methods for Stochastic Computations: A Spectral Method Approach* (Princeton Univ. Press, 2010).
105. Austin, A. C. M. & Sarris, C. D. Efficient analysis of geometrical uncertainty in the FDTD method using polynomial chaos with application to microwave circuits. *IEEE Trans. Microw. Theory Tech.* **61**, 4293–4301 (2013).
Provides an FDTD-based method for the modelling of geometric uncertainties.
106. Edwards, R. S., Marvin, A. C. & Porter, S. J. Uncertainty analyses in the finite-difference time-domain method. *IEEE Trans. Electromagn. Compat.* **52**, 155–163 (2010).
107. Ishimaru, A. *Electromagnetic Wave Propagation, Radiation, and Scattering: From Fundamentals to Applications* 2nd edn (John Wiley & Sons, 2017).
108. Taflove, A. & Hagness, S. C. Periodic structures. in *Computational Electromagnetics: The Finite-Difference Time-Domain Method* Ch. 13 (Artech House, Inc., 2005).
109. Chan, C. T., Yu, Q. L. & Ho, K. M. Order-N spectral method for electromagnetic waves. *Phys. Rev. B* **51**, 16635–16642 (1995).
110. Luo, C., Johnson, S. G., Joannopoulos, J. D. & Pendry, J. B. Negative refraction without negative index in metallic photonic crystals. *Opt. Express* **11**, 746–754 (2003).
111. Ward, A. J. & Pendry, J. B. Calculating photonic Green's functions using a nonorthogonal finite-difference time-domain method. *Phys. Rev. B* **58**, 7252–7259 (1998).
112. Ward, A. J. & Pendry, J. B. A program for calculating photonic band structures, Green's functions and transmission/reflection coefficients using a non-orthogonal FDTD method. *Computer Phys. Commun.* **128**, 590–621 (2000).
113. Kokkinos, T., Sarris, C. D. & Eleftheriades, G. V. Periodic finite-difference time-domain analysis of loaded transmission-line negative-refractive-index metamaterials. *IEEE Trans. Microw. Theory Tech.* **53**, 1488–1495 (2005).
114. Liu, Y., Sarris, C. D. & Eleftheriades, G. V. Triangular-mesh-based FDTD analysis of two-dimensional plasmonic structures supporting backward waves at optical frequencies. *J. Lightwave Technol.* **25**, 938–945 (2007).
115. Aminian, A., Yang, F. & Rahmat-Samii, Y. Bandwidth determination for soft and hard ground planes by spectral FDTD: a unified approach in visible and surface wave regions. *IEEE Trans. Antennas Propag.* **53**, 18–28 (2005).
116. Yang, F., Chen, J., Qiang, R. & Elsherbeni, A. A simple and efficient FDTD/PBC algorithm for scattering analysis of periodic structures. *Radio Sci.* https://doi.org/10.1029/2006rs003526 (2007).
117. Holter, H. & Steyskal, H. Infinite phased-array analysis using FDTD periodic boundary conditions-pulse scanning in oblique directions. *IEEE Trans. Antennas Propag.* **47**, 1508–1514 (1999).
118. Turner, G. M. & Christodoulou, C. FDTD analysis of phased array antennas. *IEEE Trans. Antennas Propag.* **47**, 661–667 (1999).
119. Zhao, Q. & Sarris, C. D. Discontinuous Galerkin time domain modeling of metasurface geometries with multi-rate time stepping. in *2021 IEEE MTT-S International Microwave Symposium (IMS)* (IEEE, 2021).
120. Guo, S. et al. Metalens for improving optical coherence tomography. *J. Korean Phys. Soc.* **81**, 32–37 (2022).
121. Eid, A., Winkelmann, J. A., Eshein, A., Taflove, A. & Backman, V. Origins of subdiffractional contrast in optical coherence tomography. *Biomed. Opt. Express* **12**, 3630–3642 (2021).
122. Cherkezyan, L. et al. Interferometric spectroscopy of scattered light can quantify the statistics of subdiffractional refractive-index fluctuations. *Phys. Rev. Lett.* https://doi.org/10.1103/physrevlett.111.033903 (2013).
123. Li, Y. et al. Nanoscale chromatin imaging and analysis platform bridges 4D chromatin organization with molecular function. *Sci. Adv.* **7**, eabe4310 (2021).
124. Sun, G., Fu, C., Dong, M., Jin, G. & Song, Q. The finite-difference time-domain (FDTD) guided preparation of Ag nanostructures on Ti substrate for sensitive SERS detection of small molecules. *Spectrochim. Acta Pt A: Mol. Biomolecular Spectrosc.* **269**, 120743 (2022).
125. Seo, J.-H., Han, Y. & Chung, J.-Y. A comparative study of birdcage RF coil configurations for ultra-high field magnetic resonance imaging. *Sensors* **22**, 1741 (2022).
126. Taflove, A. & Brodwin, M. E. Computation of the electromagnetic fields and induced temperatures within a model of the microwave-irradiated human eye. *IEEE Trans. Microw. Theory Tech.* **23**, 888–896 (1975).
127. Chiang, J., Wang, P. & Brace, C. L. Computational modelling of microwave tumour ablations. *Int. J. Hyperth.* **29**, 308–317 (2013).
128. Chakarothai, J., Watanabe, S. & Wake, K. Numerical dosimetry of electromagnetic pulse exposures using FDTD method. *IEEE Trans. Antennas Propag.* **66**, 5397–5408 (2018).
129. Hajiaboli, A. & Popovie, M. FDTD analysis of light propagation in the human photoreceptor cells. *IEEE Trans. Magn.* **44**, 1430–1433 (2008).
130. Arifler, D. et al. Light scattering from normal and dysplastic cervical cells at different epithelial depths: finite-difference time-domain modeling with a perfectly matched layer boundary condition. *J. Biomed. Opt.* **8**, 484–494 (2003).
131. Su, X.-T., Singh, K., Rozmus, W., Backhouse, C. & Capjack, C. Light scattering characterization of mitochondrial aggregation in single cells. *Opt. Express* **17**, 13381–13388 (2009).
132. Simpson, J. J., Capoglu, I. R. & Backman, V. Using FDTD to improve our understanding of partial wave spectroscopy for advancing ultra early-stage cancer detection techniques. in *2009 13th International Symposium on Antenna Technology and Applied Electromagnetics and the Canadian Radio Science Meeting* (IEEE, 2009).
133. Silla, G., Bastianelli, L., Colella, E., Moglie, F. & Primiani, V. M. SAR computation due to wearable devices by using high-resolution body models and FDTD numerical code. in *2022 International Symposium on Electromagnetic Compatibility — EMC Europe*. (IEEE).
134. Al-Sehemi, A., Al-Ghamdi, A., Dishovsky, N., Atanasov, N. & Atanasova, G. Miniaturized wearable antennas with improved radiation efficiency using magneto-dielectric composites. *IETE J. Res.* **68**, 1157–1167 (2022).
135. Arunkumar, R., Suaganya, T. & Robinson, S. Design and analysis of 2D photonic crystal based biosensor to detect different blood components. *Photonic Sens.* **9**, 69–77 (2019).
136. Warren, C., Giannopoulos, A. & Giannakis, I. gprMax: open source software to simulate electromagnetic wave propagation for ground penetrating radar. *Computer Phys. Commun.* **209**, 163–170 (2016).
137. Lee, H. O., Teixeira, F. L., San Martin, L. E. & Bittar, M. S. Numerical modeling of eccentered LWD borehole sensors in dipping and fully anisotropic earth formations. *IEEE Trans. Geosci. Remote Sens.* **50**, 727–735 (2012).
138. Pokhrel, S., Nguyen, B., Rodriguez, M., Bernabeu, E. & Simpson, J. J. A finite difference time domain investigation of electric field enhancements along ocean–continent boundaries during space weather events. *J. Geophys. Res. Space Phys.* **123**, 5033–5046 (2018).
139. Thevenot, M., Bérenger, J.-P., Monediere, T. & Jecko, F. A FDTD scheme for the computation of VLF-LF propagation in the anisotropic earth–ionosphere waveguide. *Ann. Telecommun.* **54**, 297–310 (1999).
140. Bérenger, J.-P. FDTD computation of VLF–LF propagation in the Earth–ionosphere waveguide. *Ann. Telecommun.* **57**, 1059–1090 (2002).
141. Bérenger, J.-P. Reduction of the angular dispersion of the FDTD method in the Earth–ionosphere waveguide. *J. Electromagn. Waves Appl.* **17**, 1225–1235 (2003).
142. Bérenger, J.-P. An implicit FDTD scheme for the propagation of VLF–LF radio waves in the Earth–ionosphere waveguide. *Comptes Rendus Phys.* **15**, 393–402 (2014).
143. Bérenger, J.-P. FDTD propagation of VLF–LF waves in the presence of ions in the Earth–ionosphere waveguide. *Ann. Telecommun.* **75**, 437–446 (2020).
144. Burns, S., Gasdia, F., Simpson, J. J. & Marshall, R. A. 3-D FDTD modeling of long-distance VLF propagation in the Earth–ionosphere waveguide. *IEEE Trans. Antennas Propag.* **69**, 7743–7752 (2021).

145. Hu, W. & Cummer, S. A. An FDTD model for low and high altitude lightning-generated EM fields. *IEEE Trans. Antennas Propag.* **54**, 1513–1522 (2006).
146. Smith, D. R., Huang, C. Y., Dao, E., Pokhrel, S. & Simpson, J. J. FDTD modeling of high-frequency waves through ionospheric plasma irregularities. *J. Geophys. Res. Space Phys.* **125**, e2019JA027499 (2020).
147. Niknam, K. & Simpson, J. A review of grid-based, time-domain modeling of electromagnetic wave propagation involving the ionosphere. *IEEE J. Multisc. Multiphys. Comput. Tech.* **6**, 214–228 (2021).
Summarizes the FDTD method applied to propagation in the ionosphere.
148. Cummer, S. A. Dynamics of causal beam refraction in negative refractive index materials. *Appl. Phys. Lett.* **82**, 2008–2010 (2003).
Uses FDTD to demonstrate the dynamic evolution of negative refraction and sub-wavelength focusing with planar negative index lenses.
149. Foteinopoulou, S., Economou, E. N. & Soukoulis, C. M. Refraction in media with a negative refractive index. *Phys. Rev. Lett.* https://doi.org/10.1103/physrevlett.90.107402 (2003).
150. Kokkinos, T., Islam, R., Sarris, C. D. & Eleftheriades, G. V. Rigorous analysis of negative refractive index metamaterials using FDTD with embedded lumped elements. in *2004 IEEE MTT-S International Microwave Symposium Digest* (IEEE Cat. No. 04CH37535) (IEEE, 2004).
151. Li, D. & Sarris, C. D. A unified FDTD lattice truncation method for dispersive media based on periodic boundary conditions. *J. Lightwave Technol.* **28**, 1447–1454 (2010).
152. Pendry, J. B. Negative refraction makes a perfect lens. *Phys. Rev. Lett.* **85**, 3966–3969 (2000).
153. Taflove, A., Oskooi, A. & Johnson, S. G. *Advances in FDTD Computational Electrodynamics: Photonics and Nanotechnology* (Artech House, 2013).
A perspective on advanced FDTD algorithms in the context of photonics and nanotechnology.
154. Chen, Z., Taflove, A. & Backman, V. Photonic nanojet enhancement of backscattering of light by nanoparticles: a potential novel visible-light ultramicroscopy technique. *Opt. Express* **12**, 1214–1220 (2004).
This paper uses FDTD to discover the existence of photonic nanojets.
155. Karamehmedović, M., Scheel, K., Listov-Saabye Pedersen, F., Villegas, A. & Hansen, P.-E. Steerable photonic jet for super-resolution microscopy. *Opt. Express* **30**, 41757–41773 (2022).
156. Prather, D. W. & Shi, S. Formulation and application of the finite-difference time-domain method for the analysis of axially symmetric diffractive optical elements. *J. Opt. Soc. Am. A* **16**, 1131–1142 (1999).
157. Tong, M.-S. et al. Analysis of photonic band-gap (PBG) structures using the FDTD method. *Microw. Opt. Technol. Lett.* **41**, 173–177 (2004).
158. Sánchez-Postigo, A. et al. Breaking the coupling efficiency–bandwidth trade-off in surface grating couplers using zero-order radiation. *Laser Photon. Rev.* **15**, 2000542 (2021).
159. Lavrinenko, A. V., Novitsky, A. & Zhilko, V. V. ARROW-based silicon-on-insulator photonic crystal waveguides with reduced losses. *Opt. Quantum Electron.* **38**, 815 (2007).
160. Bahadori, M., Nikdast, M., Cheng, Q. & Bergman, K. Universal design of waveguide bends in silicon-on-insulator photonics platform. *J. Lightwave Technol.* **37**, 3044–3054 (2019).
161. Kedia, J. & Gupta, N. An FDTD analysis of serially coupled double ring resonator for DWDM. *Optik* **126**, 5641–5644 (2015).
162. Gray, S. K. & Kupka, T. Propagation of light in metallic nanowire arrays: finite-difference time-domain studies of silver cylinders. *Phys. Rev. B* https://doi.org/10.1103/physrevb.68.045415 (2003).
163. Oubre, C. & Nordlander, P. Optical properties of metallodielectric nanostructures calculated using the finite difference time domain method. *J. Phys. Chem. B* **108**, 17740–17747 (2004).
164. Zeng, Z., Venuthurumilli, P. K. & Xu, X. Inverse design of plasmonic structures with FDTD. *ACS Photon.* **8**, 1489–1496 (2021).
165. Ludwig, A., Sarris, C. D. & Eleftheriades, G. V. Metascreen-based superdirective antenna in the optical frequency regime. *Phys. Rev. Lett.* https://doi.org/10.1103/physrevlett.109.223901 (2012).
166. Gabay, D., Yilmaz, A., Boag, A. & Natan, A. Modeling electromagnetic wave phenomena in large quantum systems: formulation and computational costs. *IEEE Antennas Propag. Mag.* **63**, 29–39 (2021).
167. Martin, R. M. *Electronic Structure: Basic Theory and Practical Methods* (Cambridge Univ. Press, 2004).
168. Sholl, D. S. & Steckel, J. A. *Density Functional Theory* (John Wiley & Sons, Ltd, 2009).
169. Payne, M. C., Teter, M. P., Allan, D. C., Arias, T. A. & Joannopoulos, J. D. Iterative minimization techniques for ab initio total-energy calculations: molecular dynamics and conjugate gradients. *Rev. Mod. Phys.* **64**, 1045–1097 (1992).
170. Chew, W. C., Liu, A. Y., Salazar-Lazaro, C. & Sha, W. E. Quantum electromagnetics: a new look — part I. *IEEE J. Multisc. Multiphys. Comput. Tech.* **1**, 73–84 (2016).
171. Chew, W. C., Liu, A. Y., Salazar-Lazaro, C. & Sha, W. E. Quantum electromagnetics: a new look — part II. *IEEE J. Multisc. Multiphys. Comput. Tech.* **1**, 85–97 (2016).
172. Fox, A. M. & Fox, M. *Quantum Optics: An Introduction* Vol. 15 (Oxford Univ. Press, 2006).
173. Gerry, C., Knight, P. & Knight, P. L. *Introductory Quantum Optics* (Cambridge Univ. Press, 2005).
174. Miller, D. A. B. *Quantum mechanics for scientists and engineers* (Cambridge University Press, 2008).
175. Na, D.-Y. & Chew, W. C. Quantum electromagnetic finite-difference time-domain solver. *Quantum Rep.* **2**, 253–265 (2020).
176. Na, D.-Y., Zhu, J. & Chew, W. C. Diagonalization of the Hamiltonian for finite-sized dispersive media: canonical quantization with numerical mode decomposition. *Phys. Rev. A* **103**, 063707 (2021).
177. Na, D.-Y., Zhu, J., Chew, W. C. & Teixeira, F. L. Quantum information preserving computational electromagnetics. *Phys. Rev. A* **102**, 013711 (2020).
178. Thiel, W., Tornquist, K., Reano, R. & Katehi, L. P. B. A study of thermal effects in RF-MEM-switches using a time domain approach. in *2002 IEEE MTT-S International Microwave Symposium Digest* (Cat. No. 02CH37278) (IEEE, 2002).
179. Alsunaidi, M. A., Imtiaz, S. M. S. & El-Ghazaly, S. M. Electromagnetic wave effects on microwave transistors using a full-wave time-domain model. *IEEE Trans. Microw. Theory Tech.* **44**, 799–808 (1996).
180. Grondin, R. O., El-Ghazaly, S. M. & Goodnick, S. A review of global modeling of charge transport in semiconductors and full-wave electromagnetics. *IEEE Trans. Microw. Theory Tech.* **47**, 817–829 (1999).
181. Piket-May, M. et al. High-speed electronic circuits with active and nonlinear components. in *Computational Electrodynamics: The Finite-Difference Time-Domain Method* Ch. 15 (Artech House, Inc., 2005).
182. Sui, W., Christensen, D. A. & Durney, C. H. Extending the two-dimensional FDTD method to hybrid electromagnetic systems with active and passive lumped elements. *IEEE Trans. Microw. Theory Tech.* **40**, 724–730 (1992).
183. Decleer, P. & Vande Ginste, D. A hybrid EM/QM framework based on the ADHIE-FDTD method for the modeling of nanowires. *IEEE J. Multisc. Multiphys. Comput. Tech.* **7**, 236–251 (2022).
184. Hue, Y.-K., Teixeira, F. L., Martin, L. S. & Bittar, M. S. Three-dimensional simulation of eccentric LWD tool response in boreholes through dipping formations. *IEEE Trans. Geosci. Remote Sens.* **43**, 257–268 (2005).
185. Zhang, Y., Simpson, J. J., Welling, D. & Liemohn, M. Improving the efficiency of Maxwell's equations FDTD modeling for space weather applications by scaling the speed of light. in *2020 IEEE USNC-CNC-URSI North American Radio Science Meeting (Joint with AP-S Symposium)* (IEEE, 2020).
186. Sarris, C. D. Extending the stability limit of the FDTD method with spatial filtering. *IEEE Microw. Wirel. Compon. Lett.* **21**, 176–178 (2011).
187. Jandhyala, V., Michielssen, E. & Mittra, R. FDTD signal extrapolation using the forward–backward autoregressive (AR) model. *IEEE Microw. Guided Wave Lett.* **4**, 163–165 (1994).
188. Nayak, I., Kumar, M. & Teixeira, F. L. Detection and prediction of equilibrium states in kinetic plasma simulations via mode tracking using reduced-order dynamic mode decomposition. *J. Comput. Phys.* **447**, 110671 (2021).
189. Smith, D. R., Tan, T., Dao, E., Huang, C. & Simpson, J. J. An FDTD investigation of orthogonality and the backscattering of HF waves in the presence of ionospheric irregularities. *J. Geophys. Res. Space Phys.* https://doi.org/10.1029/2020ja028201 (2020).
190. Donderici, B. & Teixeira, F. L. Domain-overriding and digital filtering for 3-D FDTD subgridded simulations. *IEEE Microw. Wirel. Compon. Lett.* **16**, 10–12 (2006).
191. Wagner, C. L. & Schneider, J. B. Divergent fields, charge, and capacitance in FDTD simulations. *IEEE Trans. Microw. Theory Tech.* **46**, 2131–2136 (1998).
192. Schuhmann, R. & Weiland, T. Stability of the FDTD algorithm on nonorthogonal grids related to the spatial interpolation scheme. *IEEE Trans. Magn.* **34**, 2751–2754 (1998).
193. Wang, S. & Teixeira, F. L. Some remarks on the stability of time-domain electromagnetic simulations. *IEEE Trans. Antennas Propag.* **52**, 895–898 (2004).
194. Douvalis, V., Hao, Y. & Parini, C. Stable non-orthogonal FDTD method. *Electron. Lett.* **40**, 850–851 (2004).
195. Teixeira, F. L. Lattice Maxwell's equations. *Prog. Electromagn. Res.* **148**, 113–128 (2014).
196. Glasser, A. S. & Qin, H. Generalizing Yee's method: scalable geometric higher-order FEEC algorithms for Maxwell's equations on an unstructured mesh. Preprint at https://doi.org/10.48550/arXiv.2301.01753 (2023).
197. Teixeira, F. L. & Chew, W. C. Lattice electromagnetic theory from a topological viewpoint. *J. Math. Phys.* **40**, 169–187 (1999).
198. Nikolova, N. K., Tam, H. W. & Bakr, M. H. Sensitivity analysis with the FDTD method on structured grids. *IEEE Trans. Microw. Theory Tech.* **52**, 1207–1216 (2004).
199. Zhao, Q. & Sarris, C. D. Space–time adaptive modeling and shape optimization of microwave structures with applications to metasurface design. *IEEE Trans. Microw. Theory Tech.* **70**, 5440–5453 (2022).
200. Hughes, T. W., Minkov, M., Liu, V., Yu, Z. & Fan, S. A perspective on the pathway toward full wave simulation of large area metalenses. *Appl. Phys. Lett.* **119**, 150502 (2021).
201. Zivari, A. et al. On-chip distribution of quantum information using traveling phonons. *Sci. Adv.* **8**, eadd2811 (2022).
202. Balsara, D. S. & Simpson, J. J. Making a synthesis of FDTD and DGTD schemes for computational electromagnetics. *IEEE J. Multisc. Multiphys. Comput. Tech.* **5**, 99–118 (2020).
203. Sarris, C. D. Adaptive mesh refinement for time-domain numerical electromagnetics. in *Synthesis Lectures on Computational Electromagnetics* Vol. 1, 1–154 (Morgan & Claypool Publishers, 2007).
204. Huang, Z., Demarest, K. R. & Plumb, R. G. An FDTD/MoM hybrid technique for modeling complex antennas in the presence of heterogeneous grounds. *IEEE Trans. Geosci. Remote Sens.* **37**, 2692–2698 (1999).

205. Wang, Y., Safavi-Naeini, S. & Chaudhuri, S. K. A hybrid technique based on combining ray tracing and FDTD methods for site-specific modeling of indoor radio wave propagation. *IEEE Trans. Antennas Propag.* **48**, 743–754 (2000).
206. Chen, Z., Wang, C.-F. & Hoefer, W. J. R. A unified view of computational electromagnetics. *IEEE Trans. Microw. Theory Tech.* **70**, 955–969 (2022).
207. Joannopoulos, J. D., Johnson, S. G., Winn, J. N. & Meade, R. D. *Photonic Crystals: Molding the Flow of Light* 2nd edn (Princeton Univ. Press, 2008).

Acknowledgements
F.L.T. acknowledges support from the US Department of Energy Grant No. DE-SC0022982 through the NSF/DOE Partnership in Basic Plasma Science and Engineering. Part of the material from J.J.S. is based on work supported by the National Science Foundation under Grant No. 1662318. C.S. acknowledges support from the Natural Sciences and Engineering Research Council of Canada (NSERC) through a Discovery Grant. The authors acknowledge the help of K. Niknam in the generation of Fig. 5e using input data provided by T. Reichler.

Author contributions
Introduction (F.L.T., Y.Z. and J.J.S.); Experimentation (F.L.T., C.S., J.-P.B., M.O. and J.J.S.); Results (F.L.T., C.S. and J.J.S.); Applications (F.L.T., C.S., Y.Z., D.-Y.N., J.-P.B., Y.S., V.B., J.J.S. and W.C.C.); Reproducibility and data deposition (C.S., Y.Z. and J.J.S.); Limitations and optimizations (F.L.T., Y.Z. and J.J.S.); Outlook (C.S., Y.Z., D.-Y.N., J.J.S. and W.C.C.); Overview of the Primer (all authors).

Competing interests
The authors declare no competing interests.

Additional information
Peer review information *Nature Reviews Methods Primers* thanks Theodoros Zygiridis, Jiefu Chen, Jun Shibayama, Stephen Gedney and Zhizhang Chen for their contribution to the peer review of this work.

Publisher's note Springer Nature remains neutral with regard to jurisdictional claims in published maps and institutional affiliations.

Related links
Message passing interface: https://www.open-mpi.org/
OpenMP: https://www.openmp.org/resources/